On the hypothesized outflow control of tropical cyclone intensification

Michael T. Montgomery[a]*, John Persing[a], and Roger K. Smith[b]

[a] *Dept. of Meteorology, Naval Postgraduate School, Monterey, CA*

[b] *Meteorological Institute, Ludwig Maximilians University of Munich, Munich, Germany*

*Correspondence to: Prof. M. T. Montgomery, Naval Postgraduate School, 589 Dyer Rd., Root Hall, Monterey, CA 93943. E-mail: mtmontgo@nps.edu

We present idealized, three-dimensional, convection-permitting numerical experiments to evaluate the premise of the revised theory of tropical cyclone intensification proposed by Emanuel (2012). The premise is that small-scale turbulence in the upper tropospheric outflow layer determines the thermal stratification of the outflow and, in turn, an amplification of the system-scale tangential wind field above the boundary layer. The aim of our paper is to test whether parameterized small-scale turbulence in the outflow region of the developing storm is an essential process in the spin up of the maximum tangential winds.

Compared to the control experiment in which the small-scale, shear-stratified turbulence is parameterized in the usual way based on a Richardson number criterion, the vortex in a calculation without a parameterized representation of vertical mixing above the boundary layer has similar evolution of intensity. Richardson number near-criticality is found mainly in the upper-level outflow. However, the present solutions indicate that eddy processes in the eyewall play a significant role in determining the structure of moist entropy surfaces in the upper-level outflow. In the three-dimensional model, these eddy processes are largely realizations of asymmetric deep convection and are not obviously governed by any Richardson number-based criterion. The experiments do not support the premise on which the new theory is based. The results would appear to have ramifications for recent studies that invoke the new theory.

Key Words: Tropical cyclone, hurricane, typhoon, spin-up

Received January 4, 2019; Revised ; Accepted

Citation: . . .

1. Introduction

The steady-state hurricane model formulated by Emanuel (1986) has been a corner stone in underpinning the theory of hurricane behaviour for the last three decades. In particular, it has formed the basis for constructing a theory for the maximum Potential Intensity (PI) that a storm may achieve at a particular location. In PI theory, intensity is defined as the maximum gradient wind at the top of the frictional boundary layer. Over the years, the model has been refined in several ways (Emanuel 1988, 1995; Bister and Emanuel 1998) and it has been extended to provide a theory for storm intensification (Emanuel 1997, hereafter E97). An appraisal of the steady-state model and its application to PI theory is provided by Montgomery and Smith (2017, see section 5). An appraisal of the unsteady version of the model and its relation to other paradigms for hurricane intensification, including a new alternative rotating-convection paradigm, is given by Montgomery and Smith (2014).

The E97 intensification theory highlighted the fronto-genetic nature of eyewall formation, drawing upon the presumed (p. 1019) " ... crucial presence of downdrafts

by reducing the entropy tendency there (outside the radius of maximum tangential wind (RMW), our insertion) by a factor β". The factor β is assumed to be a function of radius. The key element of the time-dependent model was the derivation of an expression for the time rate-of-change of the tangential wind at the top of the boundary layer (his Eqn. [20]). This expression equates the tangential wind tendency to the sum of three terms. One of these terms is always negative definite, one vanishes at the radius of maximum gradient wind (RMW), and the third is positive only if the radial gradient of the '*ad hoc*' function, $\beta(r)$, is sufficiently negative to offset the other two terms. The function $\beta(r)$ is introduced to "... crudely represent the effects of convective and large-scale downdrafts, which import low θ_e ([equivalent potential temperature - our insertion) air into the subcloud layer" (p.1019, below Eqn. (16) of E97). One problem with the theory is the lack of a rigorous basis for the formulation of $\beta(r)$. A second problem is the assumption that the boundary layer is in approximate gradient wind balance. As discussed in Smith et al. (2008), this assumption is difficult to defend in the inner-core region of a tropical cyclone.

In a series of idealized, cloud-permitting numerical experiments, Montgomery et al. (2009) showed that tropical cyclone intensification does not require downdrafts, unlike the E97 theory. Further, they showed that vortex intensification proceeds optimally in the pseudo-adiabatic case in which downdrafts are excluded altogether. These results call into question the so-called β formulation of tropical cyclone intensification. They show also that the widely held Wind-Induced-Surface-Heat-Exchange (WISHE) evaporation-wind feedback mechanism of tropical cyclone intensification is neither essential nor the dominant pathway of intensification in the prototype problem for intensification (see Section 2a).

A few years ago, Emanuel and Rotunno (2011) and Emanuel (2012) questioned the assumption of Emanuel's earlier hurricane models (the steady model of Emanuel (1986) and the time-dependent E97 model) that the air parcels rising in the eyewall exit in the lower stratosphere in a region of approximately constant absolute temperature. To quote Emanuel (2012, p. 989): "Emanuel and Rotunno (2011) demonstrated that in numerically simulated tropical cyclones, the assumption of constant outflow temperature is poor and that, in the simulations, the outflow temperature increases rapidly with angular momentum." These authors proposed a revised theory[1] postulating that "the entropy stratification is determined by a requirement that the Richardson number not fall below a critical value" and that the temperature stratification of the outflow is determined by small-scale, shear-stratified turbulence.

Ordinarily, the critical Richardson number demarcates the local boundary between stratified shear stability and instability/turbulence[2]. Here it seems that small-scale turbulence in the outflow layer is presumed to operate and bound the Richardson number to a near critical value.

In the revised intensification theory of Emanuel (2012), small-scale, shear-stratified turbulence in the upper-tropospheric outflow layer is presumed to determine the thermal stratification of the upper-level outflow and, in turn, an amplification of the system-scale tangential wind field above the boundary layer. The new theory represents a major shift in the way a storm is presumed to be influenced by its environment. In the earlier models, it was assumed that the near-isothermal structure of the lower stratosphere set the (constant) outflow temperature. In the revised time-dependent theory, the vertical structure of the outflow temperature is determined internally within the vortex so that, in principal, it no longer matches the temperature structure of the storm environment. While the revised steady-state theory of Emanuel and Rotunno (2011) was configured to ensure that the outflow temperature at the radius of maximum wind (in angular momentum coordinates) equals the temperature of the environment (p2245)[3], the time-dependent theory does not appear to impose such a constraint.

A key result of the revised analytical intensification theory of Emanuel (2012) (see his section 3) is the derivation of a new expression for the time rate-of-change of tangential wind (his Eqn. [16]) (analogous to Eqn. 20 of E97). The right-hand side of this tendency equation involves three terms: the first term vanishes at the radius of maximum gradient wind; the third term is always negative definite and can only contribute to spin down; the second term is positive and must represent a generalized Coriolis force that depends on "the radial gradient of outflow temperature, which in turn, according to the results of Part I (Emanuel and Rotunno - our insertion), is a result of small-scale turbulence in the outflow region[4]."

On the face of it, the premise of the new intensification theory as articulated above appears implausible to us, at least from a fluid dynamics perspective, because of the tenuous link between small-scale mixing processes in the upper tropospheric outflow layer and the amplification of the system scale swirling wind at the top of the boundary layer. While the new theory makes numerous assumptions (some of which are highlighted later), to us the purported nature of this tangential force is the most mysterious facet of the revised theory. Another puzzling assumption used to generate solutions presented by Emanuel (2012), was the choice of an unrealistically large value of 5000 m for the boundary layer depth, h.

For the foregoing reasons an immediate question arises as to whether or not the premise of the new theory is physically defensible, at least for realistic parameter values

[1] In the revised theory, the maximum gradient wind is reduced by a factor of approximately $1/\sqrt{2}$ compared with the nominal potential intensity when the ratio of the bulk enthalpy exchange and drag coefficient is near unity ($C_k/C_D = 1$). The reduced intensity is a consequence of neglecting the pressure dependence of the saturation mixing ratio in the theory (see Emanuel and Rotunno 2011, pp. 2246-47).

[2] In fluid dynamics, a Richardson number of 0.25 defines the instability threshold for normal mode disturbances in the absence of moist processes (Drazin and Reid 1981). When turbulent processes are allowed for, the criticality boundary is usually extended to a value of unity based on simple energetics considerations (e.g., Cushman-Roisin 1994). In the revised steady state and intensification theories, this criticality boundary is tacitly assumed to hold true when moist processes are included.

[3] "... a shooting method is applied in which an outer radius [r_o - our insertion] is first specified, the system [defined by thier Equations (31) and (35) - our insertion] integrated, and the outflow temperature at the radius of maximum winds is noted. If it is not equal to T_t [the ambient tropopause temperature - our insertion], the integration is restarted with a new value of r_o, and so on, until the outflow temperature at the radius of maximum winds equals T_t".

[4] Later for pedagogical purposes we review in Appendix A the key assumptions and approximations underlying the new tendency equation and we derive the tendency equation from these assumptions. The derivation exposes *inter alia* the tangential force that is responsible for increasing the maximum tangential wind at the top of the boundary layer in the new theory.

consistent with the latest observational guidance? This question is relevant in view of recent studies that invoke the revised theory for the determination of a universal tangential wind profile for a hurricane (Chavas and Lin 2016) and as support for the integrity of a redefined Wind-Induced-Surface-Heat-Exchange (WISHE) intensification theory (Zhang and Emanuel 2016). The question is relevant also because the Emanuel (2012) theory has been invoked recently to suggest that tropical cyclones will be more prone to rapid intensification in a warmer climate, with the rate of storm intensification scaling as the square of the potential intensity (Emanuel 2017).

As an additional remark, it is worth pointing out that, because of the underlying axisymmetric formulation of the revised intensification theory, the hypothesis of small-scale, shear-stratified turbulence control on *vortex intensification* tacitly assumes that the shear stratified turbulence can be meaningfully represented as ring-like eddy structures encircling the vortex axis. In reality, such turbulent mixing occurs locally in azimuth and the axisymmetric assumption is highly questionable. Moreover, given the intrinsic limitations of vortex intensification in strict axisymmetric geometry in comparison with companion three-dimensional simulations (Persing et al. 2013), one should have a healthy skepticism for an axisymmetric theory of vortex spin up that invokes small-scale mixing processes in the upper troposphere to produce a generalized Coriolis force in the tangential direction to spin up the maximum tangential wind, which occurs at the top of the boundary layer. For these reasons, we will not use an axisymmetric model and use instead a three-dimensional model as the proper benchmark to evaluate the premise of the revised intensification theory.

We defer further discussion of the foregoing issues until later after we have summarized the results of two idealized, three-dimensional, experiments designed to test the new outflow control premise on vortex intensification for realistic parameter settings based on the latest observational guidance.

In the next section we describe the setup of the numerical experiments that are used to test the premise of the new intensification theory. The key results are discussed in Section 3 and a discussion of these and conclusions are the topic of Section 4.

2. The Model and Experiments

2.1. *Model core and pertinent parameter settings*

The model configuration relates to the prototype problem for tropical cyclone intensification. This problem considers the evolution of an initially cloud free, axisymmetric vortex of near tropical storm strength in thermal wind balance, embedded in a mean tropical environment without any ambient flow. The simulations are carried out using the numerical model of Bryan and Fritsch (2002), CM1 version 14. The reference sounding is the near-neutral sounding of Rotunno and Emanuel (1987). A detailed listing of the common and relevant numerical parameters and their definitions in the FORTRAN code is provided in Appendix B.

The simplest physics options are chosen to provide the cleanest possible comparison to the idealized framework of Emanuel (2012)'s new axisymmetric intensification theory. The effects of radiation are represented by Newtonian damping towards the reference sounding, with the damping rate capped at 2 K day^{-1}. The upper boundary includes a Rayleigh damping layer in the height range 20-25 km to control gravity wave noise reflected from the top boundary. Precipitation is represented by the simple scheme of Rotunno and Emanuel (1987) with a fixed fall speed for liquid water of 7 m s^{-1}. Ice microphysical processes are neglected. The foregoing options, while arguably difficult to justify for prolonged (multiple week) simulations (Persing et al. 2018), are adequate to simulate the intensification of an initial cyclonic vortex for the prototype problem on a realistic forecast time scale of order 5 days.

The calculations are carried out on an f-plane with the Coriolis parameter $f = 5 \times 10^{-5}$ s^{-1}, corresponding to 20°N. The sea surface temperature is fixed at 299.3 K (26.15 C).

2.2. *Sub grid-scale turbulence parameterization*

A bulk aerodynamic formulation for heat and enthalpy is used to model the turbulent momentum and enthalpy transfer at the sea surface and, for simplicity, the generally wind-speed dependent values of these exchange coefficients are taken to be constant. The enthalpy transfer coefficient is $C_k = 1.29 \times 10^{-3}$ and the drag coefficient is $C_{\rm D} = 2.58 \times 10^{-3}$. These constant values of surface exchange coefficients represent the best mean estimates from the latest in-situ observations under major hurricane conditions (Bell et al. 2012a).

The subgrid-scale turbulence is represented by choosing option "iturb=3" in the model, which is designed for problems that do not resolve any part of the turbulent Kolmogorov inertial range. This choice requires the specification of the horizontal mixing length $l_{\rm h} = 700$ m and the vertical mixing length $l_{\rm v} = 50$ m. These values are based on the recent observational findings of Zhang and Montgomery (2012) and Zhang et al. (2011b), respectively, and the resulting vertical and horizontal eddy diffusivities that are output in the model simulations. These values are also close to the values recommended by Bryan (2012) in order to produce realistic hurricane structure. For simplicity, these mixing lengths are assumed constant in both space and time.

The subgrid scale scheme follows the traditional formulation of Smagorinsky (1963) and Lilly (1962), except that different eddy viscosities are employed for the horizontal and vertical directions. As per the CM1 documentation, the flow-dependent momentum diffusivities in the horizontal and vertical directions are specified as follows: $K_{\rm m,h} = l_{\rm h}^2 S_{\rm h}$ and $K_{\rm m,v} = l_{\rm v}^2 S_{\rm v} \sqrt{1 - {\rm Ri}/{\rm Pr}}$, where the m subscript refers to momentum and the second subscript h or v refer to the horizontal and vertical directions, $S_{\rm h}$ and $S_{\rm v}$ denote the parts of the total deformation, S, that involve the horizontal and vertical strain components, ${\rm Ri} = N_m^2/S_{\rm v}^2$ is the moist Richardson number, N_m^2 is the moist Brunt-Väisälä frequency, and Pr is the Prandtl number (set to unity in this option) (see Bryan and Fritsch (2002) for complete definitions of these parameters). In this scheme, the heat and momentum diffusivities are taken to be identical, i.e. $K_{\rm h} = K_{\rm m}$ and the vertical eddy diffusivity is proportionally reduced in regions with positive moist Richardson number (< 1). Whenever Ri exceeds unity, $K_{\rm h,v}$ and $K_{\rm m,v}$ are set to zero.

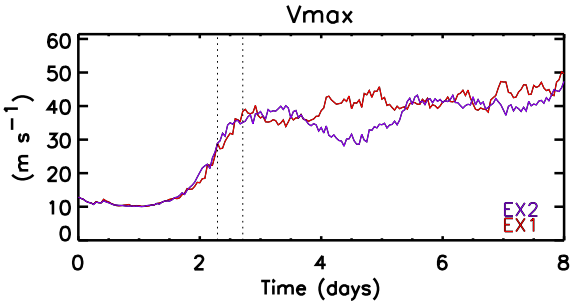

Figure 1. Time-series of maximum azimuthally-averaged tangential wind V_{max} for the control experiment EX-1 (red) and from the suppressed vertical diffusivity experiment EX-2 (blue) ($K_v = 0$ everywhere above 1 km height). The period 55 to 65 h is shown by dotted lines.

2.3. *Initial conditions*

The same initial cyclonic vortex is used for both simulations. The initial radial and vertical velocity are set to zero. The initial tangential velocity and temperature fields are in thermal wind balance (see appendix for further details). This tangential velocity has a maximum of 13 m s^{-1} at the surface at a radius of 100 km radius. It varies smoothly in space, declining to zero at a radius of 400 km radius, beyond which it is set to zero. It is set to zero also above a height of 20 km. Appendix B gives the mathematical formula for the tangential wind as per the CM1 model code and displays its radius-height structure.

2.4. *The experiments*

The control experiment, EX-1, is like the three-dimensional 3D3k simulation described by Persing et al. (2013) (with the same horizontal grid spacing described there, see Appendix B), except with a fixed vertical grid spacing of 250 m, so as to provide good resolution of the outflow layer (and a little better resolution than the 312.5 m grid spacing simulations employed by Emanuel and Rotunno (2011). Experiment EX-2 is similar to EX-1, but it is designed to suppress sub-grid scale mixing in the vertical direction above the boundary layer. Here, the vertical diffusivity K_v is set equal to zero at each time step above a height of 1 km. The suppression of vertical mixing by sub grid scale turbulence short circuits any presumed link between small-scale turbulence above the boundary layer and the amplification of tangential wind on the vortex scale. This remark applies, in particular, to parameterized small-scale turbulence in the upper-troposphere. If the new intensification theory of Emanuel (2012) is correct, then the vortex with zero vertical mixing should not intensify.

3. Results from idealized numerical experiments

3.1. *Vortex intensification compared*

Figure 1 shows a time series over an 8 day interval of the azimuthally-averaged maximum tangential velocity in the main experiments, EX-1 and EX-2. This time interval spans more than a typical forecast time scale of 3 to 5 days. The evolution of wind intensity until 90 hours is approximately the same in both simulations[5]. During this time the vortices intensify rapidly with a maximum spin up rate of around 1 m s^{-1} h^{-1} at 55 hours. After 72 h, barring fluctuations comparable in magnitude to the variability reported in Nguyen et al. (2008), the vortices continue to intensify with a reduced time-mean rate and achieve peak intensities of 50 m s^{-1} at 8 days.

3.2. *Outflow temperature evolution*

Figure 2 shows radius-time plots of the azimuthally-averaged temperature deviation from the environmental temperature near 11 km height in EX-1 and EX-2. The 11 km height is chosen because it corresponds approximately to the level where the Richardson number is most-frequently critical (see below). This height is where the shear-stratified (parameterized turbulent) mixing is hypothesized to have an important influence on the thermal and angular momentum structure of the vortex. The far-field environmental temperature at this altitude is 230.9 K, and remains near its initial value for the full simulation.

During the time interval covering the gestation and rapid intensification periods of the vortex (0 to 3 d), both experiments exhibit a progressively growing warm anomaly ($>$ 2K) inside a 50 km radius. Beyond this radius, the warm anomaly diminishes in strength until the 800 km radius where the outflow jet terminates (not shown). Emanuel's revised intensification theory presumes a modification of the thermal stratification of the air that emerges from the eyewall. In turn, this thermal structure controls the spin up of the vortex below. In EX-2, without vertical subgrid scale mixing, the evolution of the outflow temperature through rapid intensification (0 to 3 days) is very similar to that of EX-1. Beyond 3 days, the evolution of the outflow temperature exhibits more temporal fluctuation.

To investigate the possible dependence of the upper-tropospheric lapse rate on the parameterized vertical mixing, Figure 3 shows the deviation of the upper-level lapse rate from the environment for both the control (EX-1) and zero diffusivity experiment (EX-2). As above, the same height (11 km) is chosen for these lapse rate calculations. The lapse rate deviation within a radius of approximately 150 km shows a similar evolution for both experiments EX-1 and EX-2 through the bulk of the rapid intensification interval (0 to 2.5 days). After this time, the lapse rate deviation for EX-2 may be described as having somewhat more static stability than EX-1 at this height level between 100 and 1,000 km radius. At these longer times, specific events in EX-1 showing less static stability (more negative values in the figure) can be traced to outward propagating features that move with a radial speed of approximately 300 km day^{-1} (3.4 m s^{-1}). This diagnosis suggests that the radial structure of evolving lapse rate may be more-readily explained by outward advection of discrete features generated from the eyewall than a local subgrid scale mixing parameterization in the outflow region exterior to the eyewall.

In summary, the static stability in EX-2 is broadly similar to EX-1, but with generally greater stability. With static stability serving here as a proxy of $\partial s^{\star}/\partial M$, one must expect some difference in the simulated intensity evolution of EX-2 relative to EX-1, but this is not found in Figure 1.

[5]For all of the experimental results presented here, the term 'intensity' is used in a more general sense than in PI theory and is defined as the azimuthally-averaged maximum tangential velocity. This maximum generally occurs in the frictional boundary layer at a height of approximately 600 m.

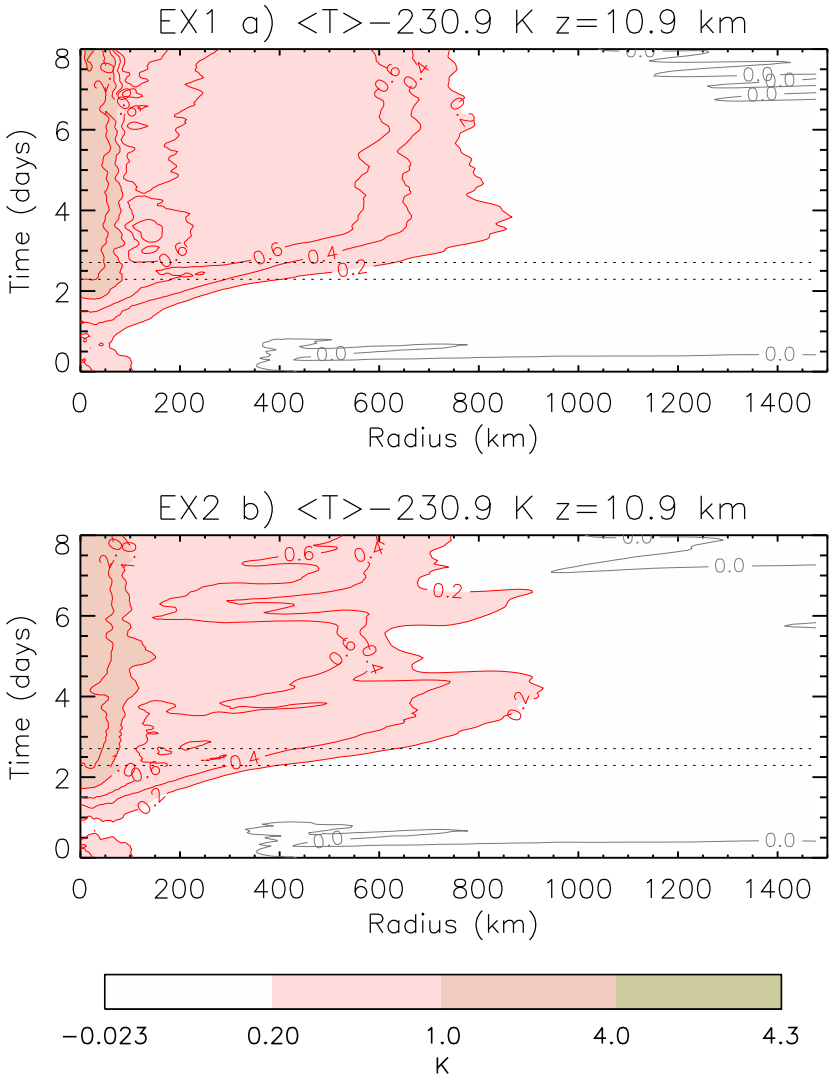

Figure 2. Radius-time contour plots of azimuthally-averaged temperature deviation from the far-field at 10.9 km height. The far-field temperature at this height is 230.9 K. Contours shown are $\pm\{0.2, 0.4, 0.6, 1.0, 2.0, 4.0\}$ K. Red contours denote positive values and blue contours denote negative values. Shading indicated in color bar. Top panel (a) for the control experiment EX-1, bottom panel (b) for experiment EX-2. The data shown are smoothed in time using a 5 hour boxcar smoother. The rapid intensification period spanning 55 to 65 h is highlighted by dotted lines.

3.3. *Richardson number structure*

In the CM1 model, the shear-stratified turbulence parameterization scheme is activated when the Richardson number has a value between zero and one. The gradient Richardson number in this model is implemented in Cartesian coordinates as follows

$$\mathrm{Ri_{CM1}} = \frac{N_\mathrm{m}^2}{2\left(\frac{\partial w}{\partial z}\right)^2 + \left(\frac{\partial w}{\partial x} + \frac{\partial u_x}{\partial z}\right)^2 + \left(\frac{\partial w}{\partial y} + \frac{\partial u_y}{\partial z}\right)^2}, \quad (1)$$

with u_x, u_y, and w being the components of the wind in the x-, y-, and z-directions, respectively. Here, we evaluate this quantity in storm-centered cylindrical coordinates using

$$\mathrm{Ri_{CM1}} = \frac{N_\mathrm{m}^2}{2\left(\frac{\partial w}{\partial z}\right)^2 + \left(\frac{1}{r}\frac{\partial w}{\partial \lambda} + \frac{\partial v}{\partial z}\right)^2 + \left(\frac{\partial w}{\partial r} + \frac{\partial u}{\partial z}\right)^2}, \quad (2)$$

where u, v, and w are the r-, λ-, and z-components of the velocity vector, respectively, and N_m^2 is the local moist static stability as computed by the numerical model (Durran and Klemp 1982). In the diagnosis presented here, the Richardson number is computed locally at every grid point on a (r, λ, z, t) grid, at one-hour intervals between 55 and 65 hours, during the rapid intensification phase (see Fig. 1)[6]. Figure 4 shows the azimuthal-time average of $\mathrm{Ri_{CM1}}$ during this period for experiments EX-1 and EX-2. It shows also the relative frequency at which criticality (1.0 or below) occurs in each experiment at each (r, z) point within the 360 degree azimuth and during the 10 hour time averaging interval.

During the rapid intensification period in the control simulation, criticality is found (Fig. 4a) in the time-azimuth mean below the outflow around 11 km height and outside 60 km radius. A similar analysis for EX-2 (Fig. 4b) shows about the same extent of criticality. The low-level eyewall in both EX-1 and EX-2 has large spatial shears in the

[6]For the computation of $\mathrm{Ri_{CM1}}$ shown here, the potential temperature, pressure, vapor and liquid mixing ratios, and tangential and radial wind components are interpolated to the cylindrical grid from the original Cartesian computational grid. The Richardson number is computed at each point on the cylindrical grid at each time, and then averaged.

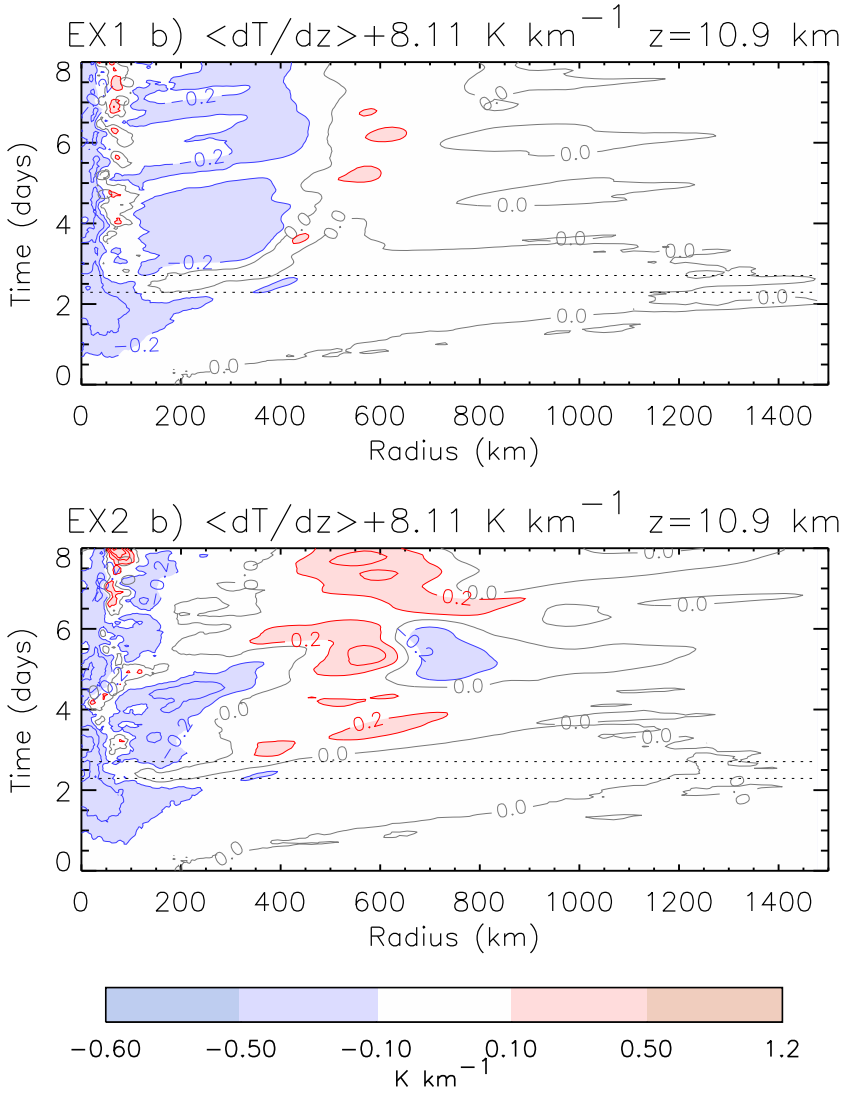

Figure 3. Radius-time contour plots of azimuthally-averaged lapse rate deviation from the far-field at 10.9 km height. The far-field lapse rate at this height is -8.11 K km^{-1}. Contours are shown with an interval of 0.1 K km^{-1}. Blue contours denote lapse rates that are greater (more negative) than the far-field and red contours denote lapse rates smaller (less negative) than the far-field. Shading indicated in the color bar. Top panel (a) for the control experiment EX-1, bottom panel (b) for experiment EX-2. The data shown are smoothed in time using a 5-hour boxcar smoother. The rapid intensification period spanning 55 to 65 h is highlighted by dotted lines.

flow, from which near-critical values of Richardson number are found extending up to 2 km height. The mid-level has relatively larger values of Richardson number. Frequencies of occurrence of criticality greater than 50% (red in Figs. 4c,d) are limited to the identified regions, above and below the upper-level outflow jet and in the low-level eyewall, plus a layer in middle of the planetary boundary layer at 500 m height.

3.4. Is there a relation between upper-level mixing and Richardson number?

Comparison of our computation of $\mathrm{Ri}_{\mathrm{CM1}}$ (Fig. 4a) with that of Figure 6a of Emanuel and Rotunno (2011) show a few differences which, for completeness, should be carefully considered. First, they display $\sqrt{\mathrm{Ri}}$. Second, they compute Richardson number based on the 24 hour averaged fields from an axisymmetric model versus our display of the time-azimuth average of Richardson number computed locally in space and time. Third, Emanuel and Rotunno (2011) display values from the mature stage, while we show values from the rapid intensifying stage (55-65 h). Our Figure 4a shows a region of criticality in the outflow region similar to that of Emanuel and Rotunno (2011) using the same metric[7]. We can confirm the large region of negative values of Ri through the mid-to-lower troposphere when we performed a separate computation with the Emanuel and Rotunno (2011) formula, hereafter $\mathrm{Ri}_{\mathrm{ER11}}$[8]. In the tropical atmosphere, one would expect to find a reversal of sign with height of $\partial s^*/\partial z$ (vertical gradient of saturated entropy, e.g. Holton 2004, Fig 11.1). The mean of $\mathrm{Ri}_{\mathrm{CM1}}$ does not show such a region of negative values through the mid-to-lower troposphere as does $\mathrm{Ri}_{\mathrm{ER11}}$. This difference is

[7]Our previous paper Persing et al. (2013) provided a preliminary analysis of the Richardson number in three-dimensional and axisymmetric hurricane simulations. We discovered a coding error in our previous diagnosis of the gradient Richardson number that over-reported the value of this number. This error has been corrected here.

[8]We presume that Emanuel and Rotunno (2011) also computed negative values of $\mathrm{Ri}_{\mathrm{ER11}}$, and that as an expedient they have displayed imaginary values of $\sqrt{\mathrm{Ri}_{\mathrm{ER11}}}$ as zero.

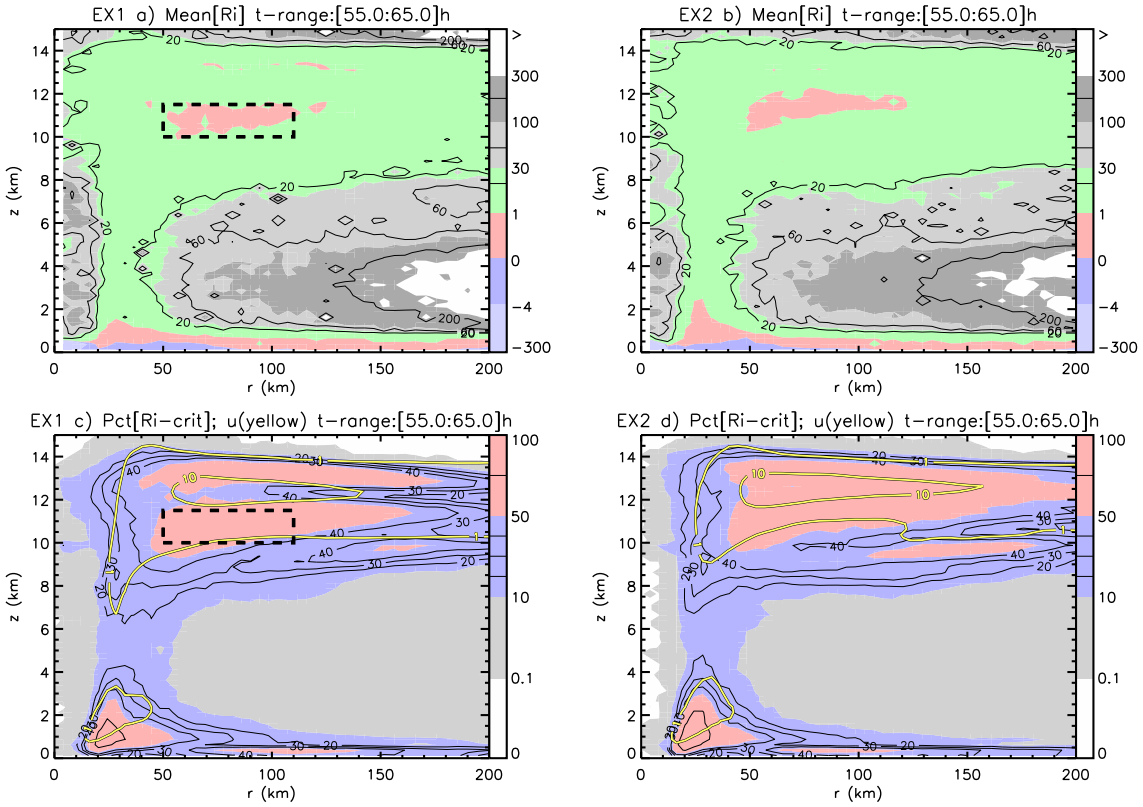

Figure 4. Panels (a) and (b) show radius-height structure of azimuthal-time-mean gradient Richardson number $\mathrm{Ri}_{\mathrm{CM1}}$ for experiments EX-1 and EX-2, respectively. Values are shown by shading indicated in the color bar. Supplemental contours of 20, 60, and 200 are shown also. Panels (c) and (d) show the relative frequency ('PCT') of occurrence of $0 \leq \mathrm{Ri}_{\mathrm{CM1}} \leq 1$ (marking criticality) at each (r, z) coordinate during the time intervals $55 \leq t \leq 65$ h. Frequency is shown by shading indicated in the color bar. Supplemental contours of 20, 30, 40, and 75 % are shown also. The azimuthal-time mean outflow jet is indicated by the yellow curves in panels (c) and (d) with contours of 1 and 10 m s^{-1}. The dashed box denotes an annulus of criticality referred to in the text.

attributable in part to how the CM1 model uses a separate dry calculation for uncloudy grid cells and to the somewhat different formulation of N_m^2 in the cloudy cells. Where the water vapor content is small in the upper troposphere, the CM1 formulation (based on Durran and Klemp (1982)) and Emanuel and Rotunno (2011) formulation should (and do) agree.

In CM1, by design, the quantity $\mathrm{Ri}_{\mathrm{CM1}}$ controls the activation of a sub-grid scale vertical mixing parameterization when $\mathrm{Ri}_{\mathrm{CM1}} < 1$, thereby initiating subgrid scale mixing associated with shear-stratified turbulence. Activation of shear-stratified turbulence is prevalent in the outflow of EX1, but in EX2, where this process is artificially suppressed, there is essentially no significant difference in evolution of intensity from EX-1 during the main intensification period. The EX2 simulation shows greater spatio-temporal variability of the secondary circulation and in turn a more extensive region of criticality than EX1 (Fig. 4d), even as the spatio-temporal averaged $\mathrm{Ri}_{\mathrm{CM1}}$ is very similar in the outflow (Fig. 4a,b). We conclude that mixing by shear-stratified turbulence is not essential for tropical cyclone intensification in the prototype problem using standard values of the model parameters and using the latest observational guidance for horizontal and vertical turbulence mixing lengths in real tropical cyclones.

The question remains as to what degree the postulated shear-stratified turbulent signature is identifiable in the simulated CM1 data? The revised PI theory of Emanuel and Rotunno (2011) presumes subgrid scale mixing of entropy across M-surfaces to determine the outflow stratification. To examine this question, we use equivalent potential temperature θ_e as a proxy for moist entropy. Figure 5 quantifies the eddy and diffusive fluxes of θ_e that contribute to the redistribution of θ_e across M-surfaces in EX-1 for the same time period as Figure 4. All quantities plotted in this figure are time averaged over the time interval $55 \leq t \leq 65$ h for experiment EX-1 and averaged azimuthally also. Two challenges that arise in applying the Emanuel and Rotunno (2011) theory should be noted here. First, the core of the outflow jet (Fig. 5a), presumably originating from the strongest updrafts found near the radius of maximum winds, is a region of large values of Richardson number (values up to 20 in Fig. 4a), thus spoiling a basic tenet of Emanuel and Rotunno (2011). Second, the explicit assumption in Emanuel and Rotunno (2011) (p. 2243) that there is a one-to-one relationship between M and saturation entropy is violated in the simulation by the folding of the M-surfaces at various levels of the outflow jet (Fig. 5c,d).

As evident in Figure 4, there is an annulus of criticality where $\mathrm{Ri}_{\mathrm{CM1}}$ is predominantly less than one ($50 \leq r \leq 110$ km, $10 \leq z \leq 11.5$ km). Accordingly, in this region one would expect to find some footprint of the proposed mixing process. In Figure 4c, we see that this annulus is located in the outflow jet below the jet maximum. The two principal signals of entropy mixing are the resolved radial (Figure 5e) and resolved vertical (Figure 5f) eddy fluxes of θ_e. The corresponding diffusive flux terms (Figures 5g and 5h) are found to be at least an order of magnitude smaller (note the smaller contour values of panels g and h). The resolved eddy fluxes are largest near the eyewall and are of

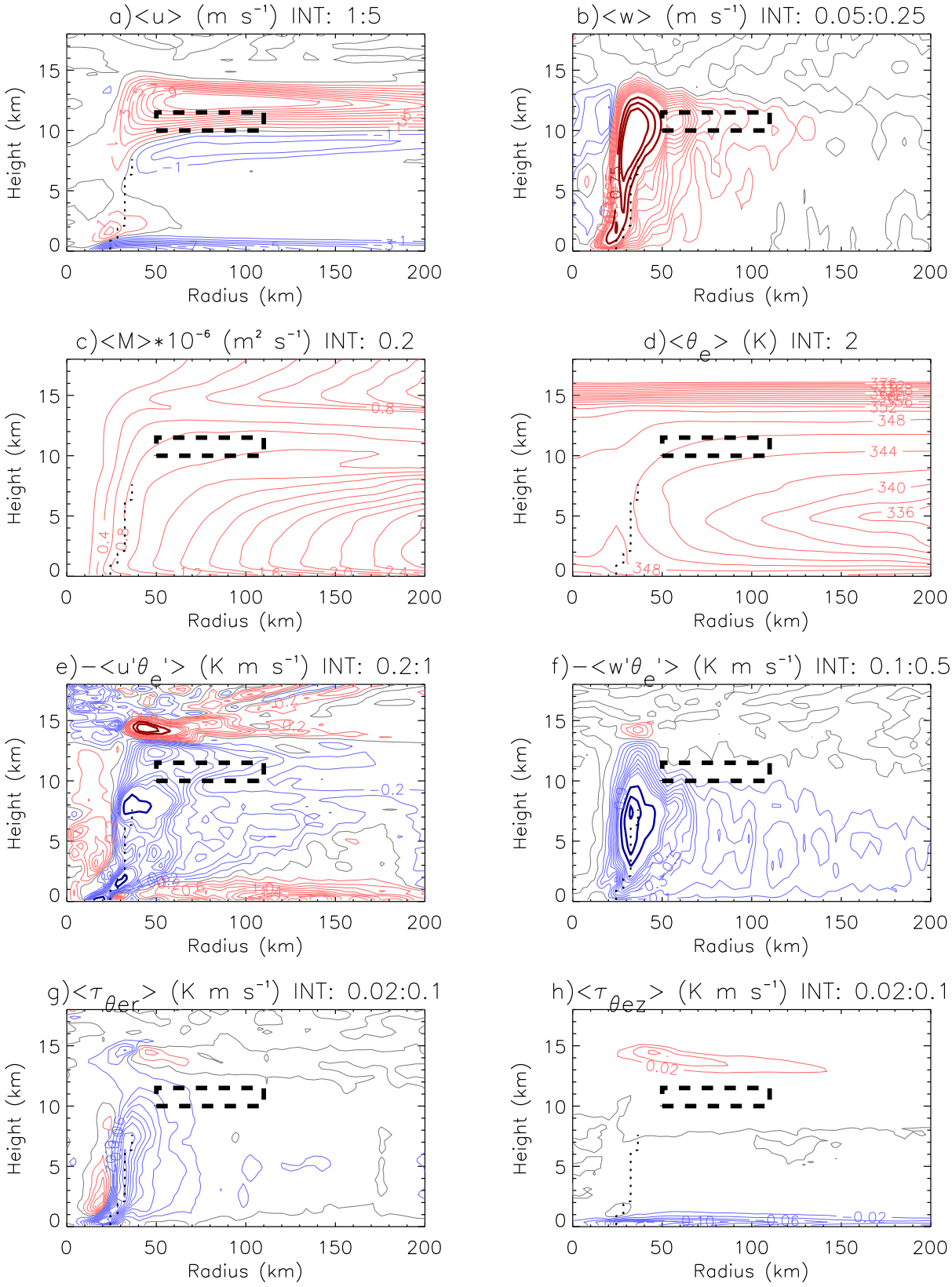

Figure 5. Contours of azimuthal-time-mean quantities (indicated by a bracket symbol) from EX-1 for a time period during vortex intensification, 55 to 65 h, plotted as a function of radius and height, with positive contours red, zero contour in grey, and negative contours in blue. The dotted curve shows the radius of the maximum azimuthally-averaged tangential wind as a function of height below 7 km height. (a) mean radial wind $\langle u \rangle$ with contour interval of 1 m s^{-1}. (b) mean vertical velocity $\langle w \rangle$ with contour interval of 0.05 m s^{-1} (thin) and 0.25 m s^{-1} (thick) beginning at 0.75 m s^{-1}. (c) mean absolute angular momentum $\langle M \rangle$, shown with values divided by 10^6, with contour interval of 0.2 m^2 s^{-1}. d) mean equivalent potential temperature $\langle \theta_e \rangle$ with contour interval of 5 K. (e) $-\langle u'\theta_e' \rangle$, the mean radial eddy flux of θ_e, with contour interval 0.2 K m s^{-1} (thin) and 1 K m s^{-1} (thick) starting at ± 3 K m s^{-1}. (f) $-\langle w'\theta_e' \rangle$, the mean vertical eddy flux of θ_e, with contour interval 0.1 K m s^{-1} (thin) and 0.5 K m s^{-1} (thick) starting at ± 1.5 K m s^{-1}. (g) $\langle \tau_{\theta_e r} \rangle$, the parameterized mean radial flux of θ_e corresponding to (e) with contour interval 0.02 K m s^{-1}. (h) $\langle \tau_{\theta_e z} \rangle$, the parameterized mean vertical flux of θ_e corresponding to (f) with contour interval 0.02 K m s^{-1}. The black dotted box is the same as that shown in Figure 4.

lesser magnitude in the upper-level outflow. Of interest also is that the Richardson-number based mixing represented by $\tau_{\theta_e z}$ shows contours above the core of the outflow jet and not in the annulus highlighted by the box; this region above the core of the outflow shows θ_e-contours connected with the stratosphere and unconnected with the planetary boundary layer. Based on these results, it would seem highly implausible that this region of subgrid scale mixing could contribute to the spin up of the vortex at the top of the boundary layer as presumed in Emanuel (2012).

On the basis of the foregoing evidence, it would seem that the rearrangement of entropy occurs mainly in the eyewall region. Moreover, Ri-criticality, which is limited to the outflow, bears little relation to this rearrangement process. The identified eddy processes in the eyewall are largely realizations of asymmetric deep convection in the model and are not obviously governed by any Richardson number-based criterion.

4. Discussion and conclusions

We have used two idealized, three-dimensional, numerical experiments to evaluate the premise of the revised theory of tropical cyclone intensification proposed by Emanuel (2012). In the revised theory, small-scale turbulence in the upper tropospheric outflow layer is hypothesized to determine the distribution of moist entropy and thermal stratification of the outflow and, in turn, *an amplification of the system-scale tangential wind field above the boundary layer*.

As noted in the Introduction, there are intrinsic differences between the behaviour of tropical cyclone vortices in axisymmetric and three-dimensional configurations (e.g. Persing et al. 2013). Since small-scale, shear-stratified turbulence is a local phenomenon and one that is not well approximated by axisymmetric rings, one should be cautiously skeptical of results from axisymmetric simulations that project this process into axisymmetric rings. The three dimensional model should be regarded as the proper benchmark.

Compared to the control experiment in which the small-scale, shear-stratified turbulence is parameterized in the usual way based on a standard Richardson number criterion, the vortex in a calculation without any representation of vertical diffusion above the boundary layer evolves in a similar way with no significant difference in the intensification rate of the maximum azimuthally-averaged tangential velocity, upper-level outflow temperature, or outflow thermal stratification.

Despite the statement of Emanuel (2012) that "... the critical Richardson number hypothesis leads to predictions of storm evolution that are also, for the most part, in good accord with (axisymmetric, our insertion) numerical simulations", our three-dimensional calculations using plausibly realistic values of the subgrid-scale turbulence parameters do not support the revised theory. Indeed, they cast strong doubt on the premise of this theory that small-scale, shear-stratified turbulence in the upper-level outflow of the developing vortex controls the intensification of the vortex. Even if the upper-tropospheric mixing leads to a generalized Coriolis force at the top of the layer with friction, which is shown in the Appendix to be at the heart of the revised intensification theory, it does not appear to manifest itself in the control experiment for realistic subgrid scale parameters.

We have offered an explanation for the different conclusions from the different numerical models and Richardson number closure formulations used by Emanuel (2012) and the present study. For the three-dimensional experiment with parameterized mixing, the rearrangement of moist entropy is found to occur mainly in the eyewall region. The diagnosed eddy processes in the eyewall are largely realizations of asymmetric deep convection in the model and are not obviously governed by any Richardson number-based criterion.

These findings are believed to be significant in the light of recent studies that invoke the revised theory for the determination of a universal tangential wind profile in hurricanes and as support for the integrity of a redefined Wind-Induced-Surface-Heat-Exchange (WISHE) intensification theory.

Acknowledgements

MTM and JP acknowledge the support of NSF grant AGS-1313948, NOAA HFIP grant N0017315WR00048, NASA grant NNG11PK021, ONR grant N0001417WX00336, and the U. S. Naval Postgraduate School. RKS acknowledges financial support from the German Research Council (Grant SM30-23) and the Office of Naval Research Global (Grant N62909-15-1-N021). The views expressed herein are those of the authors and do not represent sponsoring agencies or institutions. The data used in this paper can be accessed by emailing the first author at: mtmontgo@nps.edu.

Appendix A: Derivation of revised tendency equation and azimuthal force

Here we review the key approximations and assumptions underpinning the tendency equation the revised intensification theory of Emanuel (2012, hereafter E12). In particular, we derive the tendency equation from the stated assumptions[9]. The derivation exposes the tangential force that is responsible for amplifying the maximum tangential wind at the top of the boundary layer in the new axisymmetric theory. Amidst the derivation, some additional questions arise about the theory and its proffered analytical solution.

The starting point of the revised theory is the axisymmetric equation for the depth-averaged boundary layer moist entropy s_b in absolute angular momentum ($M = rv + 1/2fr^2$) and pressure coordinates (Eq. (12) in E12):

$$h\frac{\partial s_b}{\partial \tau} - C_{\rm D} r|\mathbf{V}|V\frac{\partial s_b}{\partial M} = C_k|\mathbf{V}|(s_0^* - s_b) + C_{\rm D}\frac{|\mathbf{V}|^3}{T_s}, \tag{3}$$

where $C_{\rm D}$ and C_k are the surface exchange coefficients for momentum and enthalpy, $\mathbf{V}$ is the Reynolds-averaged velocity vector averaged across the boundary layer, s_0^* is the saturation moist entropy (defined below) at the sea surface temperature, T_s, and h is the boundary layer depth, assumed

[9] Although we accept here the basic assumptions of the E12 theory for the purposes of gaining basic understanding, this should not be interpreted as our endorsement of these assumptions when applied to real or simulated storms in a three-dimensional configuration. In particular, we would step back from endorsing the assumption of axisymmetric moist neutral flow on the grounds that intensification is intrinsically non-axisymmetric and that M and θ_e surfaces only approach a state of congruence *after* the intensification process is already well under way (Kilroy, personnal communication).

to be constant. Here τ is the dimensional time variable wherein partial derivatives with respect to τ hold M and p constant. The boundary layer depth $h = \Delta p_b/\rho g$, where Δp_b is the boundary layer depth (in pressure units), ρ is the density averaged over the boundary layer and g is the gravitational acceleration.

The two terms on the left hand side of the entropy equation are the local time tendency of s_b and the depth-averaged radial advection of s_b in M-coordinates. (The latter uses the fact that in M-coordinates the radial velocity u_M is defined by $u_M = DM/Dt$ and $hDM/Dt = -C_{\rm D} r|\mathbf{V}|V$ from the angular momentum equation integrated over the boundary layer). The right hand side of the entropy equation consists, respectively, of the bulk-aerodynamic parameterization of the vertical transfer of moist entropy between the underlying ocean and the moist air at anemometer level and a bulk representation of dissipative heating (and corresponding entropy production). By definition, radial and vertical eddy entropy and angular momentum fluxes are zero in the axisymmetric theory.

The saturation moist entropy is given by

$$s^* = c_p \ln T - R_d \ln p + \frac{L_v q_v^*}{T} \tag{4}$$

where c_p is the specific heat of dry air at constant pressure, T is the temperature, R_d is the gas constant of dry air, p is the pressure, q_v^* is the saturation water vapour mixing ratio, and L_v is the latent heat of condensation.

The quantity s_0^* denotes the saturation entropy at the sea surface temperature

$$s_0^* = c_p \ln T_s - R_d \ln p_0 + \frac{L_v q_{v0}^*}{T_s} \tag{5}$$

where p_0 is the surface pressure and q_{v0}^* is the surface saturated vapor mixing ratio. It will prove useful later to note that if we neglect the pressure dependence of s_0^* and use the environment values to evaluate this quantity, then the M derivative of s_0^* will vanish (see below for more).

The three principal approximations that are invoked to derive the tendency equation in the new theory are the following:

- (a) neglect the pressure dependence of s_0^*;
- (b) neglect dissipative heating;
- (c) approximate $|\mathbf{V}|$ and V by V_g

where V_g is the gradient wind.

In the eyewall region, moist air rises out of the boundary layer, rapidly condenses, and ascends in cloud along M surfaces (slantwise convective neutrality). Thus, along an M surface, the saturated entropy above the boundary layer is assumed equal to the originating boundary layer entropy, $s^* = s_b$, whereupon

$$V^2 = -(T_b - T_o) M \frac{\partial s^*}{\partial M}, \tag{6}$$

where T_b is the boundary layer temperature and T_o is the outflow temperature. This equation is a form of the thermal wind equation. The variation of the outflow temperature with M is then assumed to be controlled by the action of shear-stratified turbulence wherein the gradient Richardson number is bound to a near critical value

$$\frac{\partial T_o}{\partial M} = -\frac{\mathrm{Ri}_c}{r_t^2}\left(\frac{\partial s^*}{\partial M}\right)^{-1} \tag{7}$$

which is a turbulence closure assumption on the outflow. In this equation r_t denotes the radius where the gradient Richardson number first becomes critical in the outflow layer.

The moist entropy equation at the top of the boundary layer is then

$$h\frac{\partial s^*}{\partial \tau} - C_{\rm D} V M \frac{\partial s^*}{\partial M} = C_k V (s_0^* - s^*) \tag{8}$$

Now $\frac{\partial}{\partial M}$ of Eq. (8) gives

$$h\frac{\partial}{\partial \tau}\frac{\partial s^*}{\partial M} - C_{\rm D}\frac{\partial}{\partial M}\left(VM\frac{\partial s^*}{\partial M}\right) = C_k \frac{\partial}{\partial M}[V(s_0^* - s^*)] \tag{9}$$

but Eq. (6) gives

$$\frac{\partial s^*}{\partial M} = \frac{-V^2}{(T_b - T_o)}\frac{1}{M}$$

whereupon, the first term on the left hand side of Eq. (9) becomes[10]

$$-\frac{h}{M}\frac{\partial}{\partial \tau}\left(\frac{V^2}{T_b - T_o}\right) \tag{10}$$

and the second term on the left hand side becomes

$$\begin{aligned} &-C_{\rm D}\frac{\partial}{\partial M}\left(VM\frac{\partial s^*}{\partial M}\right) \\ &= C_{\rm D}\frac{\partial}{\partial M}\left(\frac{V^3}{T_b - T_o}\right) \\ &= \frac{3C_{\rm D}V^2}{T_b - T_o}\frac{\partial V}{\partial M} + C_{\rm D}V^3\frac{\partial}{\partial M}\left(\frac{1}{T_b - T_o}\right). \end{aligned} \tag{11}$$

Now E12 makes the additional approximation

$$\frac{\partial}{\partial M}\left(\frac{1}{T_b - T_o}\right) \approx \frac{1}{(T_b - T_o)^2}\frac{\partial T_o}{\partial M}$$

This approximation follows from the assumption that T_b, the temperature after integrating across the boundary layer, is assumed to be a constant in radius (and hence M).

At this point the turbulence closure assumption, Eq. (7), is applied and $\partial s^*/\partial M$ is substituted using Eq. (6) so that

$$\begin{aligned} \frac{\partial}{\partial M}\left(\frac{1}{T_b - T_o}\right) &= \frac{-1}{(T_b - T_o)^2}\frac{\mathrm{Ri}_c}{r_t^2}\left(\frac{\partial s^*}{\partial M}\right)^{-1} \\ &= \frac{-1}{(T_b - T_o)^2}\frac{\mathrm{Ri}_c}{r_t^2} \times -\frac{M(T_b - T_o)}{V^2} \\ &= \frac{M}{V^2(T_b - T_o)}\frac{\mathrm{Ri}_c}{r_t^2} \end{aligned} \tag{12}$$

The term on the right of Eq. (9) becomes

$$\begin{aligned} &C_k\frac{\partial}{\partial M}[V(s_0^* - s^*)] \\ &\quad = C_k(s_0^* - s^*)\frac{\partial V}{\partial M} + C_k V\frac{\partial}{\partial M}(s_0^* - s^*) \end{aligned} \tag{13}$$

and E12 writes the second term on the right hand side of this equation as

$$C_k V\frac{\partial}{\partial M}(s_0^* - s^*) \approx -C_k V\frac{\partial s^*}{\partial M} = \frac{C_k V^3}{M(T_b - T_o)}, \tag{14}$$

[10] Note that M is an independent variable so that $\partial M/\partial \tau = 0$.

using Eq. (6) and neglecting the pressure dependence of s_0^* (as foreshadowed above).

Collecting the terms in Eq. (9) together now gives (using (10) - (14)),

$$-\frac{h}{M}\frac{\partial}{\partial\tau}\left(\frac{V^2}{T_b-T_o}\right) = -\frac{3C_{\rm D}V^2}{T_b-T_o}\frac{\partial V}{\partial M} - \frac{C_{\rm D}VM}{(T_b-T_o)}\frac{{\rm Ri}_c}{r_t^2} + C_k(s_0^*-s^*)\frac{\partial V}{\partial M} + \frac{C_kV^3}{M(T_b-T_o)} \quad (15)$$

or, cleaning up,

$$\frac{h}{M}\frac{\partial}{\partial\tau}\left(\frac{V^2}{T_b-T_o}\right) = \frac{\partial V}{\partial M}\left[\frac{3C_{\rm D}V^2}{T_b-T_o} - C_k(s_0^*-s^*)\right] + \frac{C_{\rm D}VM}{(T_b-T_o)}\frac{{\rm Ri}_c}{r_t^2} - \frac{C_kV^3}{M(T_b-T_o)} \quad (16)$$

Multiplying the last equation by $M(T_b-T_o)/(hV)$ gives Eq. (16) of E12:

$$\frac{T_b-T_o}{V}\frac{\partial}{\partial\tau}\left(\frac{V^2}{T_b-T_o}\right) = \frac{M}{hV}\frac{\partial V}{\partial M}\left[3C_{\rm D}V^2 - C_k(T_b-T_o)(s_0^*-s^*)\right] + \frac{C_{\rm D}}{h}\frac{{\rm Ri}_c}{r_t^2}M^2 - \frac{C_k}{h}V^2 \quad (17)$$

At $V_{\rm m}$ (the maximum tangential wind), $\partial V/\partial M = 0$, whereupon Eq. (17) simplifies to

$$\frac{T_b-T_o}{V}\frac{\partial}{\partial\tau}\left(\frac{V^2}{T_b-T_o}\right) = \frac{C_{\rm D}}{h}\frac{{\rm Ri}_c}{r_t^2}M^2 - \frac{C_k}{h}V^2. \quad (18)$$

E12 (p. 992) assumes that the outflow temperature at the RMW equals the tropopause temperature, i.e., $T_o = T_t$, with the latter assumed constant in time. This implies that the time derivative of T_o vanishes at the RMW. We can thus simplify the time derivative in the foregoing equation to obtain the tangential velocity tendency equation at the RMW:

$$\frac{\partial V_m}{\partial\tau} = \underbrace{\frac{C_{\rm D}}{2h}\frac{{\rm Ri}_c}{r_t^2}M^2}_{>0} - \underbrace{\frac{C_k}{2h}V_m^2}_{>0}, \quad (19)$$

where V_m denotes the maximum tangential velocity at the top of the boundary layer.

The foregoing is a tendency equation for V_m forced by two terms on the right hand side. The first term is positive and denotes the tangential (generalized Coriolis) force per unit mass that increases V_m with time. This term is proportional to the drag coefficient and the critical gradient Richardson number. The second term is negative and arises in association with the depletion of tangential momentum in the boundary layer. Curiously, however, this second term is proportional to the enthalpy transfer coefficient C_k. One would ordinarily expect this term to be proportional to the drag coefficient $C_{\rm D}$. E12 notes however that the equation is not yet closed and argues that it is possible that the global solution dependence on C_k may be different than would be apparent solely from an examination of this term at this stage in the derivation.

E12 proceeds to make an additional (and, in our view, unsubstantiated) assumption that the RMW always lies on the same M surface. Combining this assumption with an algebraic relation deduced from the revised steady-state theory (not written here), E12 derives an analytical (closed-form) solution for the evolution of V_m (his Eq. (19))[11]. The novelty of the result notwithstanding, the apparent elegance of the analytical solution conceals the essential role of the azimuthal force in amplifying V_m.

The critical role of the tangential force may be exposed by repeating the foregoing derivation while discarding the closure equation for the outflow temperature. In this case, one obtains at the RMW

$$\frac{\partial V_m}{\partial\tau} = \frac{C_{\rm D}{V_m}^2M}{2h(T_b-T_t)}\frac{\partial T_o}{\partial M} - \frac{C_k}{2h}V_m^2, \quad (20)$$

where T_t denotes the tropopause temperature at the RMW (assumed equal to T_o and independent of time). While other outflow closures are conceivable that would, in turn, change the specification of $\partial T_o/\partial M$, if one employs the traditional Emanuel formulation of a constant outflow temperature (e.g. E97 with $\beta = 0$), then $\partial T_o/\partial M$ would be identically zero. The resulting tendency equation for V_m in this case consists only of the second term on the right hand side of Equation (20), which is negative definite. Thus without the force in the traditional formulation of the upper boundary condition, the vortex spins down! Notwithstanding this fact, we have a more fundamental issue with the physics encompassed by Equation (20). We find it puzzling how, in reality, the stratification of the outflow layer ($\partial T_o/\partial M$) would act to move the M surfaces inwards in a way to amplify the tangential wind at the top of the boundary layer. A similar remark would apply to Equation (19), in which $\partial T_o/\partial M$ has a specific parameterization.

Appendix B: Model parameters used in numerical experiments

This appendix documents the common numerical parameters used in the numerical experiments presented in this study and those parameters that relate to specific decisions made in specifying the EX-1 simulation. Although there is some repetition of material with that of Section 2, we list all of the pertinent model parameters for completeness. This documentation would allow the reader to download the numerical model and repeat the experiments presented herein. The numerical model, CM1, is publicly available at George Bryan's UCAR webpage (www2.mmm.ucar.edu/people/bryan). Version 14

[11] The closed-form solution strictly applies only for the case in which the initial tangential velocity is everywhere zero.

(CM1v14) is used in this study; most of these parameters are common to later versions of CM1, others though are no longer supported. A name list file is used to set many parameters of the simulation at the time of execution. Simulations were performed on a Red Hat Linux cluster, kernel release 2.6.32-358.13.1.e16.x86_64 dated 17 June 2013 for x86_64 architecture using the Portland Group compiler with NetCDF support.

The grid mesh is a stretched grid in the horizontal with origin at the center of the domain (*iorigin=2*). In the middle of the domain in the horizontal is a fine-mesh grid region 405 × 405 km square with fixed grid spacing of 3 km in both the x- and y-directions. The grid configuration is established in the name list file with 185 grid points in the x- and y- directions (*nx=185, ny=185*) with stretching (*stretch_x=1, stretch_y=1*), an inner grid spacing of 3 km (*dx_inner=3000.0, dy_inner=3000.0*), an outer grid spacing of 100 km (*dx_outer=100000.0, dy_outer=100000.0*), a no-stretch length of 405 km (centered on the origin at the middle of the domain) (*nos_x_len=405000.0, nos_y_len=405000.0*), and total domain size of 2980 × 2980 km (*tot_x_len=2980000.0, tot_y_len=2980000.0*).

The vertical grid mesh has 100 points (*nz=100*) on a mesh with fixed grid spacing (*stretch_z=0, dz=250.0*)).

The equations of Bryan and Fritsch (2002) with a Runge-Kutta integrator with condensation adjustment is used (*neweqts=2*). The horizontal and vertical advection use a 5th-order scheme (*hadvorder=5, vadvorder=5*) and diffusion uses the recommended 6th-order scheme with diffusion coefficient 0.04 (*difforder=6, kdiff6=0.040*) which is in addition to the parameterized turbulence below. A vertically implicit Klemp and Wilhelmson (1978) time-splitting is used for acoustic modes (*psolver=3*), with six small time steps for each large time step (*nsound=6*). The vertically-implicit acoustic solver uses an off-centering coefficient of 0.60, which is slightly forward in time (*alph=0.60*). Potential temperature is not integrated on the small time steps (*thsmall=0*). The coefficient for a divergence damper is 0.1 (*kdiv=0.10*). As discussed in section 2, parameterized turbulence is used (*iturb=3*) with vertical and horizontal mixing length scales $l_v = 50$ m and $l_h = 700$ m (*l_v=50.0, l_h=700.0*) based on the recent observational findings of Zhang et al. (2011a) and Zhang and Montgomery (2012), and the resulting vertical and horizontal eddy diffusivities that are output in the model simulations. These values are also close to the values recommended by Bryan (2012) in order to produce realistic hurricane structure.

The fixed Coriolis parameter on an f-plane is 5×10^{-5} s^{-1} (*fcor=0.00005*).

The sea-surface temperature is 26.14 C (*tsurf=299.29*) with environmental surface pressure of 1015.1 mb (*psurf=101510.0*). The use of a simple bulk aerodynamic drag scheme (*idrag=1*) requires the use of a no-slip lower and upper boundary condition (*bcturbu=3*) setting; the treatment by the bulk aerodynamic scheme of the lower boundary in the CM1 code overrides the no-slip condition there.

A zero-flux condition is imposed at the top and bottom boundary for scalars (*bcuturbs=1*); the treatment by the bulk exchange scheme of the lower boundary in the CM1 code (*isfcflx=1*) overrides the zero-flux condition. For simplicity, we employ constant values for the drag coefficient ($C_{\rm D}$) and exchange coefficient (C_k)(*cecd=1*): $C_{\rm D} = 2.58 \times 10^{-3}$ and $C_k = 1.29 \times 10^{-3}$ (*cnstcd=0.00258, cnstce=0.00129*). The value for C_k is close to the mean value (1.2×10^{-3}) derived from the Coupled Boundary Layers/Air-Sea Transfer (CBLAST) experiment (Fig. 6 of Black et al. (2007); Fig. 4 of Zhang et al. (2009)), a recent laboratory study (Fig. 1 of Haus et al. (2010)) near and slightly above marginal hurricane wind speeds, and an energy and momentum budget analysis of the lower-tropospheric eyewall region at major hurricane wind speeds (Bell et al. 2012b). The value C_D is set to be twice the enthalpy exchange coefficient $C_{\rm D} = 2 \times C_k = 2.58 \times 10^{-3}$, and is close to the estimated mean value of $C_{\rm D} = 2.4 \times 10^{-3}$ from observations derived from CBLAST for major hurricane wind speeds by Bell et al. (2012b).

Open radiative boundary conditions are used on the lateral boundaries (*wbc=2, ebc=2, sbc=2, nbc=2*) employing the Durran and Klemp (1982) scheme (*irbc=4*); the outward flux is not restricted (*roflux=0*).

Rayleigh damping is applied at the upper boundary (*irdamp=1*) above a height of 20 km (*zd=20000.0*) with an inverse e-folding time scale of $1/300$ s^{-1} (*rdalpha=3.333e-3*). Rayleigh damping is turned off at the lateral boundaries (*hrdamp=0*). Dissipative heating is not included (*idiss=0*).

The simple Rotunno and Emanuel (1987) rainfall scheme is used (*ptype=6*) with a fixed fall speed of 7 m s^{-1} (*v_t=7.0*). Positive definiteness of moisture is ensured by a redistribution of moisture from neighboring cells (*pdscheme=1*).

As an expedient for radiative cooling, we follow Rotunno and Emanuel (1987) and choose simple Newtonian relaxation to the initial basic state sounding of potential temperature (*rterm=1*).

The initial vortex (Fig. 6) is provided in the public distribution of CM1v14, using name list option *iinit=7*. We use parameters for the nominal maximum tangential wind $V = 15$ m s^{-1}, the nominal radius of maximum tangential wind $R = 82.5$ km (although in practice the wind maximum is slightly weaker and the radius of maximum tangential wind is larger than the nominal values), the outer radius $R_0 = 412.5$ km, and the upper height for the vortex of $Z = 20$ km. The initial vortex is defined over the region $(r < R_0, z < Z)$ by

$$v(r,z) = \frac{Z-z}{Z}\left\{\sqrt{V^2\frac{r}{R}\left[G(r)+\frac{f^2r^2}{4}\right]}-\frac{fr}{2}\right\}, \tag{21}$$

where

$$G(r) = \left(\frac{2R}{r+R}\right)^2 - \left(\frac{2R}{R_0+R}\right)^2 \tag{22}$$

The basic state sounding is specified from an input file (*isnd=7*). The sounding used is obtained following the method of Rotunno and Emanuel (1987) for producing a near-neutral sounding.

References

Bell, M. M., M. T. Montgomery, and K. A. Emanuel, 2012a: Air-sea enthalpy and momentum exchange atmajor hurricane wind speeds observed during CBLAST. *J. Atmos. Sci.*, **69**, 3197–3222.

Bell, M. M., M. T. Montgomery, and W. C. Lee, 2012b: An axisymmetric view of concentric eyewall evolution in Hurricane Rita (2005). *J. Atmos. Sci.*, **69**, 2414–2432.

Bister, M., and K. A. Emanuel, 1998: Dissipative heating and hurricane intensity. *Meteor. Atmos. Phys.*, **50**, 233–240.

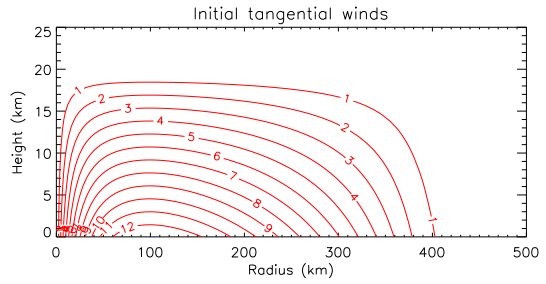

Figure 6. The initial tangential wind field (m s^{-1}) used in all numerical experiments presented.

Black, P. G., and Coauthors, 2007: Air-sea exchange in hurricanes. Synthesis of observations from the coupled boundary layer air-sea transfer experiment. *Bull Amer. Meteor. Soc.*, **88**, 357–374.

Bryan, G. H., 2012: Effects of surface exchange coefficients and turbulence length scales on the intensity and structure of numerically simulated hurricanes. *Mon. Wea. Rev.*, **140**, 1125–1143.

Bryan, G. H., and J. M. Fritsch, 2002: A benchmark simulation for moist non-hydrostatic numerical model. *Mon. Wea. Rev.*, **130**, 2917–2928.

Chavas, D. R., and N. Lin, 2016: A model for the complete radial structure of the tropical cyclone wind field. Part II: Wind field variability. *J. Atmos. Sci.*, **73**, early view.

Cushman-Roisin, B., 1994: *Introduction to Geophysical Fluid Dynamics*. Prentice Hall, 320 pp.

Drazin, P. G., and W. H. Reid, 1981: *Hydrodynamic Stability*. Cambridge University Press, Cambridge, England, 527pp.

Durran, D. K., and J. B. Klemp, 1982: On the effects of moisture on the Brunt-Väisälä frequency. *J. Atmos. Sci.*, 2152–2158.

Emanuel, K. A., 1986: An air-sea interaction theory for tropical cyclones. Part I: Steady state maintenance. *J. Atmos. Sci.*, **43**, 585–604.

Emanuel, K. A., 1988: The maximum intensity of hurricanes. *J. Atmos. Sci.*, **45**, 1143–1155.

Emanuel, K. A., 1995: Sensitivity of tropical cyclone to surface exchange coefficients and a revised steady-state model incorporating eye dynamics. *J. Atmos. Sci.*, **52**, 3969–3976.

Emanuel, K. A., 1997: Some aspects of hurricane inner-core dynamics and energetics. *J. Atmos. Sci.*, **54**, 1014–1026.

Emanuel, K. A., 2012: Self-stratification of tropical cyclone outflow. Part II: Implications for storm intensification. *J. Atmos. Sci.*, **69**, 988–996.

Emanuel, K. A., 2017: Will global warming make hurricane forecasting more difficult? *Bull. Amer. Meteor. Soc.*, **98**, 495–501.

Emanuel, K. A., and R. Rotunno, 2011: Self-stratification of tropical cyclone outflow. Part I: Implications for storm structure. *J. Atmos. Sci.*, **68**, 2236–2249.

Haus, B. K., D. Jeong, M. A. Donelan, J. A. Zhang, and I. Savelyev, 2010: Relative rates of sea-air heat transfer and frictional drag in very high winds. *Geophys. Res. Lett.*, **37**, doi:10.1029/2009GL042206, l07802.

Holton, J. R., 2004: *An Introduction to Dynamic Meteorology, 4th Edition*. Academic Press, London, 535pp.

Klemp, J. B., and R. B. Wilhelmson, 1978: The simulation of three-dimensional convective storm dynamics. *J. Atmos. Sci.*, **35**, 1070–1096.

Lilly, D. K., 1962: On the numerical simulation of buoyant convection. *Tellus*, **14**, 148–172.

Montgomery, M. T., S. V. Nguyen, R. K. Smith, and J. Persing, 2009: Do tropical cyclones intensify by WISHE? *Quart. Journ. Roy. Meteor. Soc.*, **135**, 1697–1714.

Montgomery, M. T., and R. K. Smith, 2014: Paradigms for tropical cyclone intensification. *Aust. Met. Ocean. Soc. Journl.*, **64**, 37–66.

Montgomery, M. T., and R. K. Smith, 2017: Recent developments in the fluid dynamics of tropical cyclones. *Annu. Rev. Fluid Mech.*, **49**, 541–574.

Nguyen, V. S., R. K. Smith, and M. T. Montgomery, 2008: Tropical-cyclone intensification and predictability in three dimensions. *Quart. Journ. Roy. Meteor. Soc.*, **134**, 563–582.

Persing, J., M. T. Montgomery, J. McWilliams, and R. K. Smith, 2013: Asymmetric and axisymmetric dynamics of tropical cyclones. *Atmos. Chem. Phys.*, **13**, 12 299–12 341.

Persing, J., M. T. Montgomery, R. K. Smith, and J. McWilliams, 2018: Quasi-steady hurricanes revisited. *Tropical Cyclone Science Reviews*, in press.

Rotunno, R., and K. A. Emanuel, 1987: An air-sea interaction theory for tropical cyclones. Part II Evolutionary study using a nonhydrostatic axisymmetric numerical model. *J. Atmos. Sci.*, **44**, 542–561.

Smagorinsky, J., 1963: General circulation experiments with the primitive equations. I: The basic experiment. *Mon. Wea. Rev.*, **91**, 99–164.

Smith, R. K., M. T. Montgomery, and S. Vogl, 2008: A critique of Emanuel's hurricane model and potential intensity theory. *Quart. Journ. Roy. Meteor. Soc.*, **134**, 551–561.

Zhang, F., and K. A. Emanuel, 2016: On the role of surface fluxes and wishe in tropical cyclone intensification. *J. Atmos. Sci.*, **73**, 2011–2019.

Zhang, J., W. M. Drennan, P. B. Black, and J. R. French, 2009: Turbulence structure of the hurricane boundary layer between the outer rainbands. *J. Atmos. Sci.*, **66**, 2455–2467.

Zhang, J. A., F. D. Marks, M. T. Montgomery, and S. Lorsolo, 2011a: An estimation of turbulent characteristics in the low-level region of intense Hurricanes Allen (1980) and Hugo (1989). *Mon. Wea. Rev.*, **139**, 1447–1462.

Zhang, J. A., and M. T. Montgomery, 2012: Observational estimates of the horizontal eddy diffusivity and mixing length in the low-level region of intense hurricanes. *J. Atmos. Sci.*, **69**, 1306–1316.

Zhang, J. A., R. F. Rogers, D. S. Nolan, and F. D. Marks, 2011b: On the characteristic height scales of the hurricane boundary layer. *Mon. Wea. Rev.*, **139**, 2523–2535.

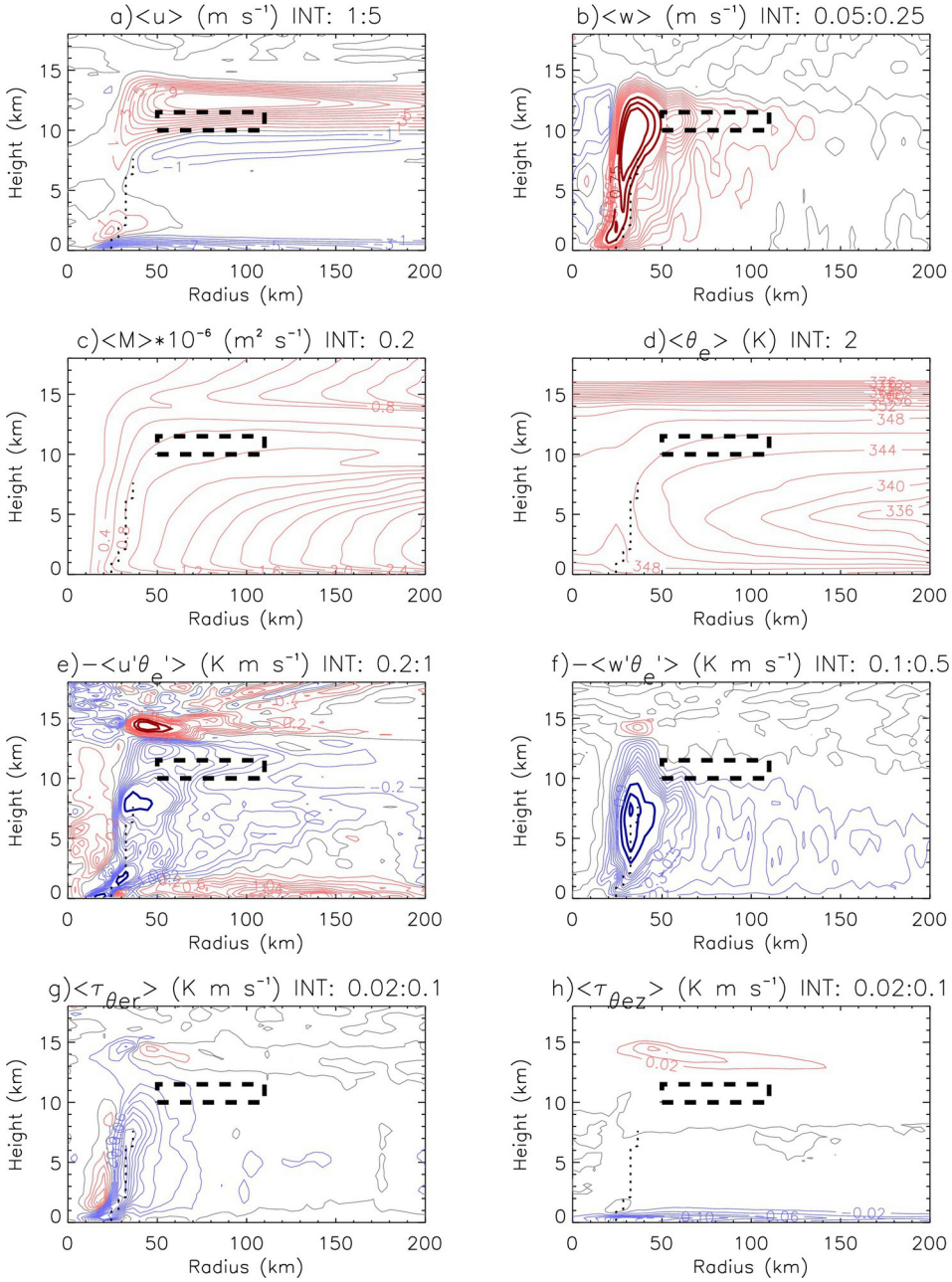

ex1_plot_eddy_thetae_m24_ex1.eps

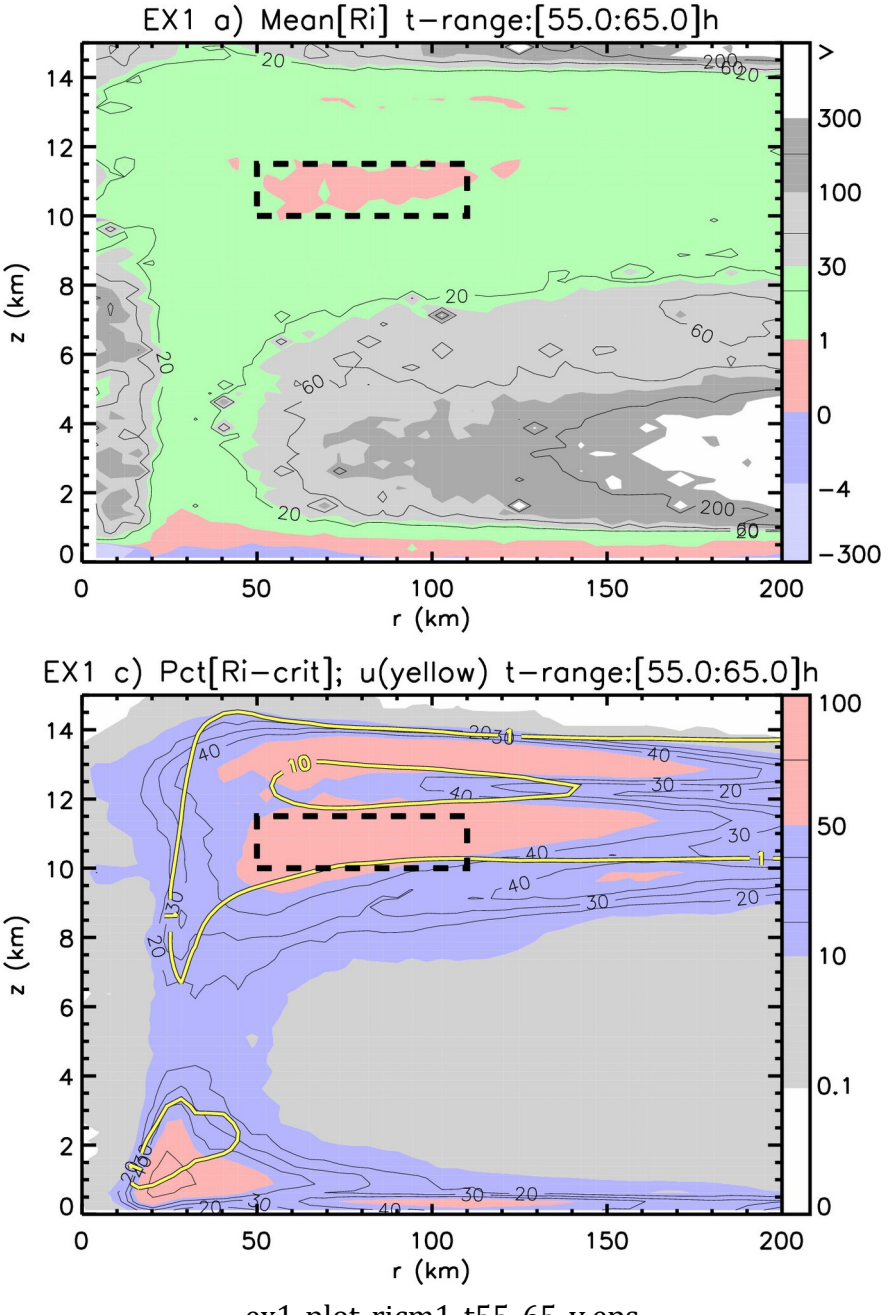

ex1_plot_ricm1_t55_65_v.eps

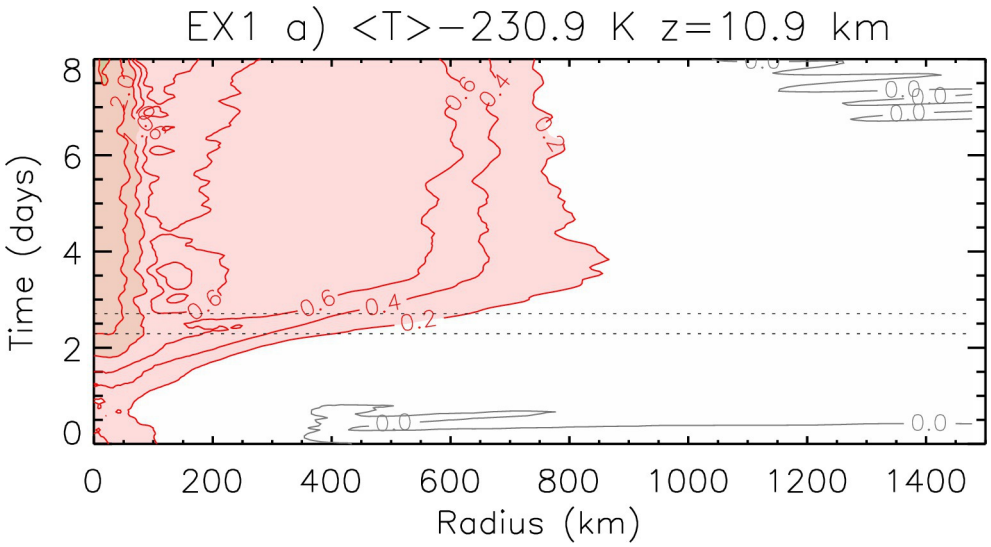

ex1_plot_rt_temperature_z43_vsr136_vst0.eps

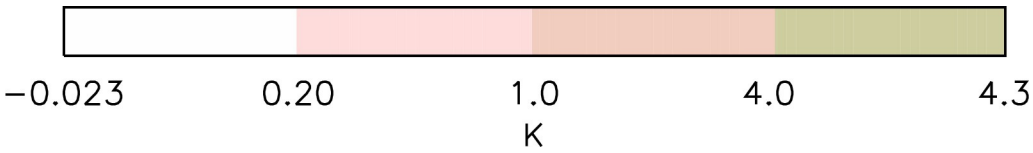

ex1_plot_rt_temperature_z43_vsr136_vst0_cbar.eps

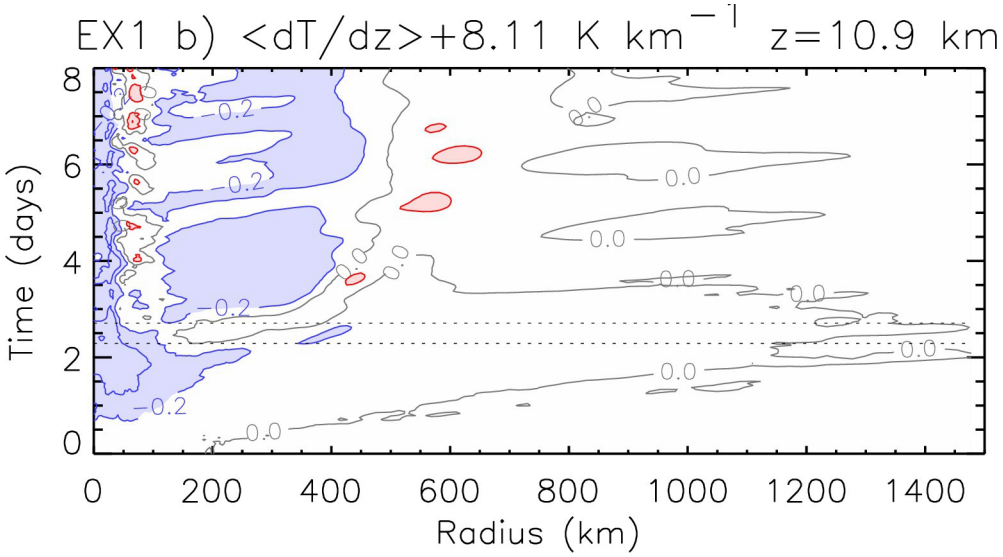

ex1_plot_rt_temperature_z43_vsr136_vst0_dtdz.eps

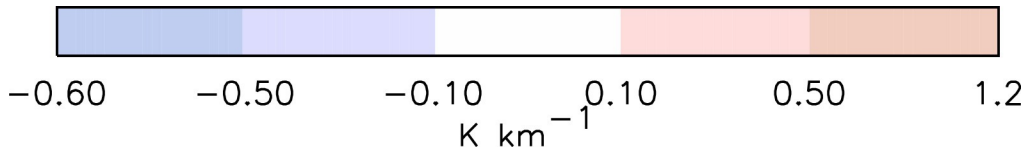

ex1_plot_rt_temperature_z43_vsr136_vst0_dtdz_cbar.eps

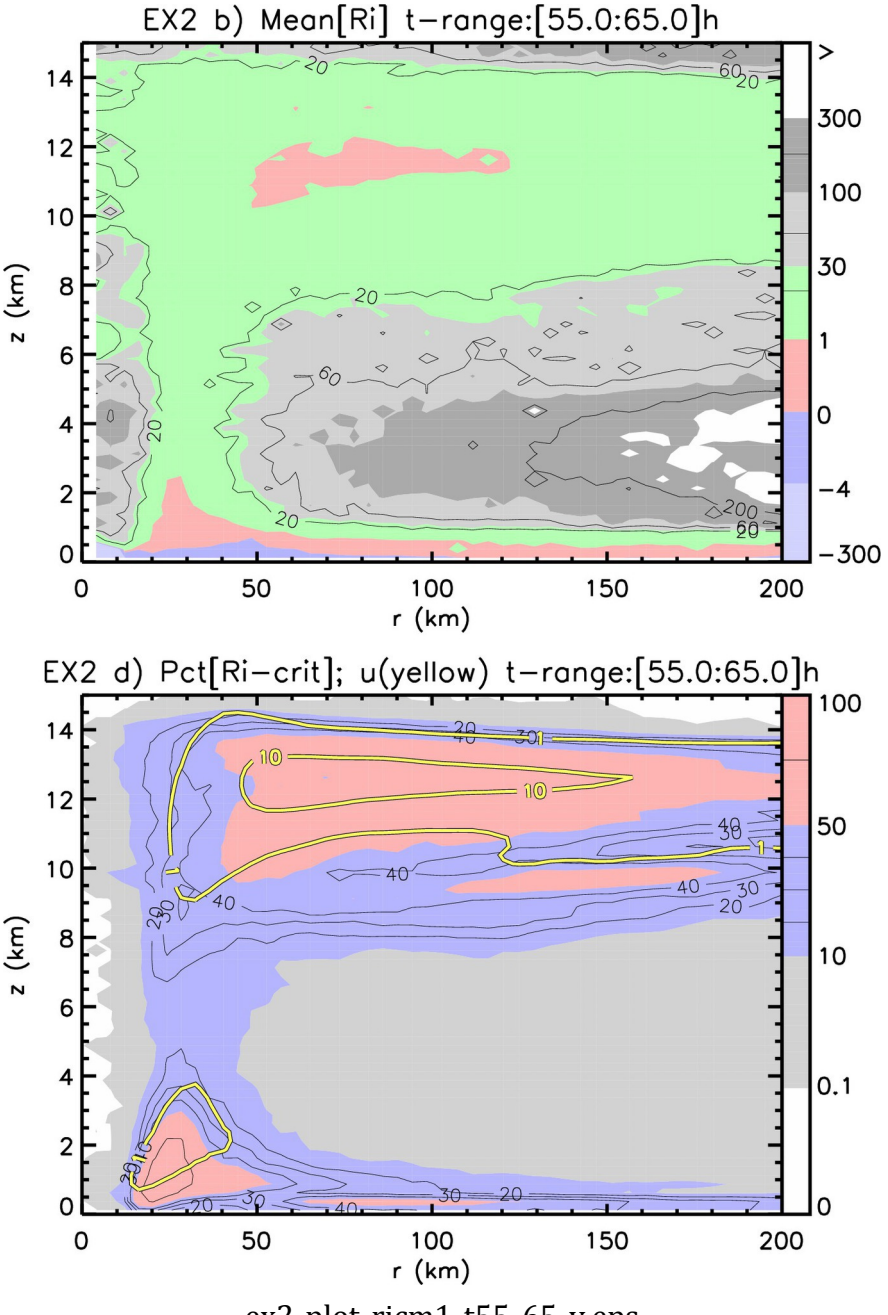

ex2_plot_ricm1_t55_65_v.eps

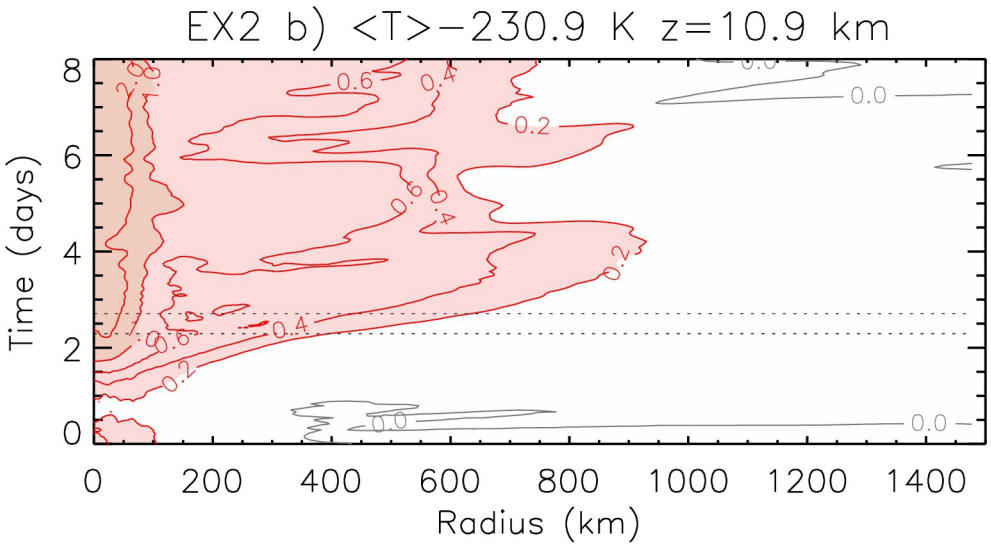

ex2_plot_rt_temperature_z43_vsr136_vst0.eps

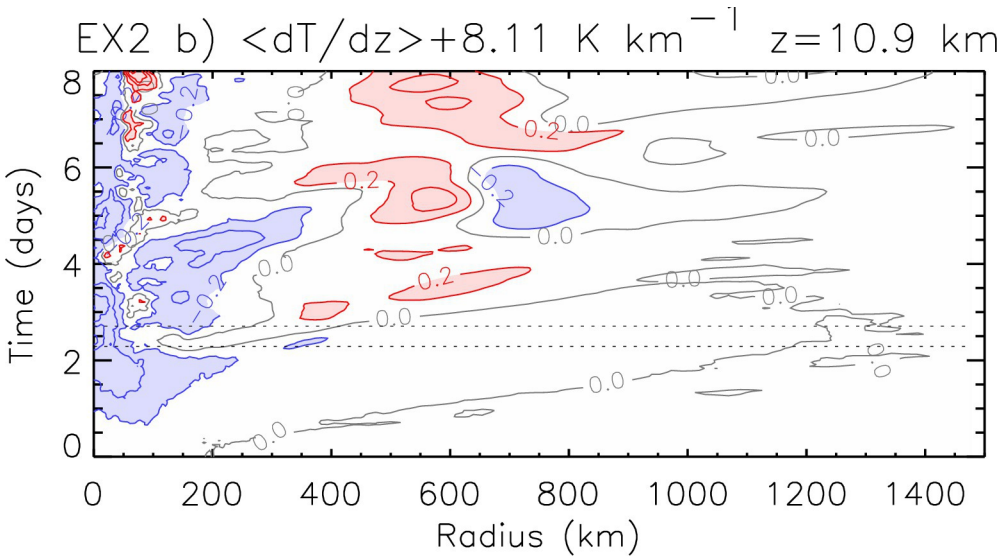

ex2_plot_rt_temperature_z43_vsr136_vst0_dtdz.eps

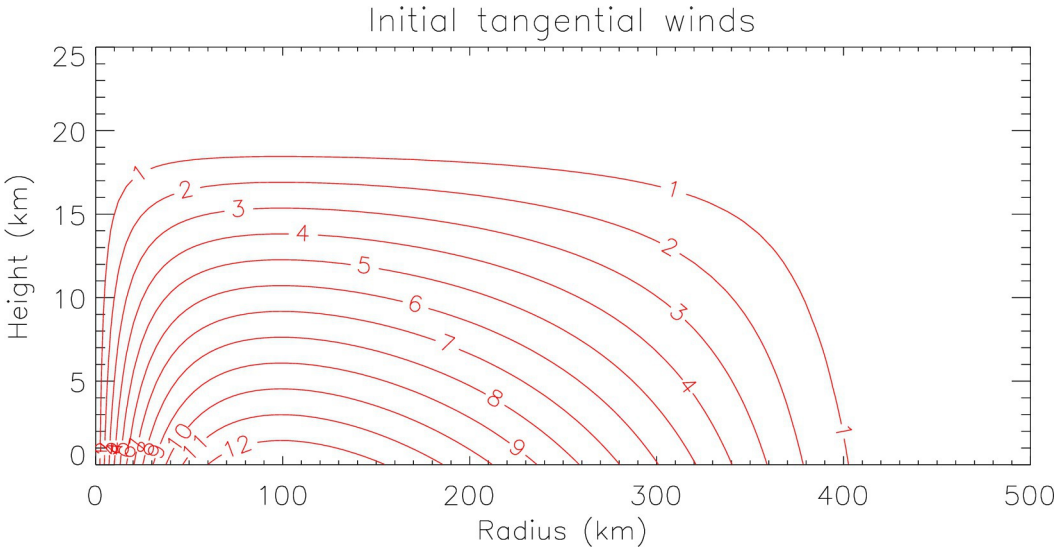

ex-2_vinit.eps

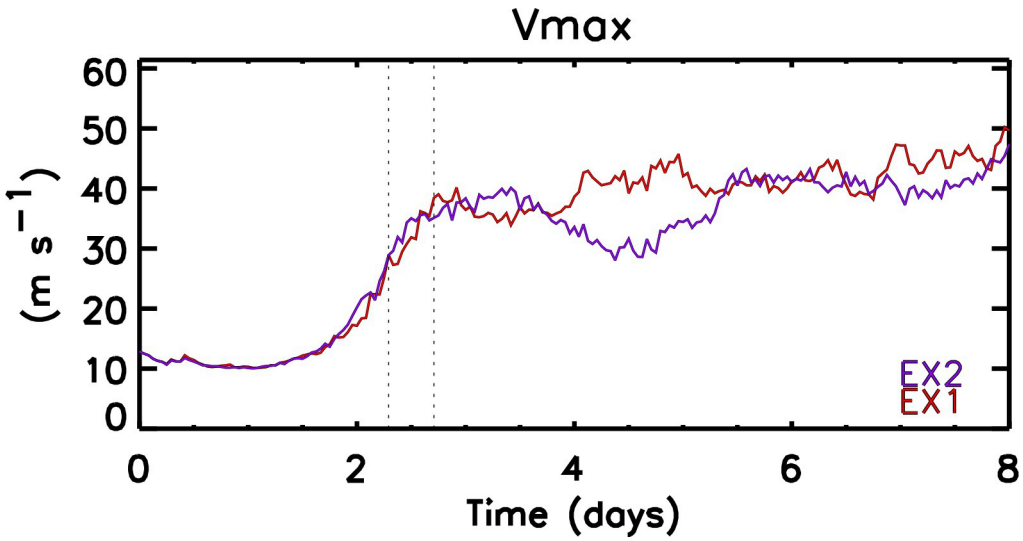

multisim_vmax_compm24_new.eps

Graphical Abstract

Title: On the Hypothesized Outflow Control of Tropical Cyclone Intensification

Lead author: Michael T. Montgomery* ; **Co-authors:** John Persing and Roger K. Smith

Key finding summary: This study evaluates the premise of Kerry Emanuel's (2012) revised theory of tropical cyclone intensification. We test the premise of the theory by conducting a control experiment with upper-level turbulence and a sensitivity experiment without upper-level turbulence. The vortex in the sensitivity experiment intensifies similar to that in the control, suggesting that upper-level mixing and the corresponding azimuthal, generalized Coriolis force are not crucial ingredients of vortex intensification in three dimensions. Physical implications of the findings are discussed.

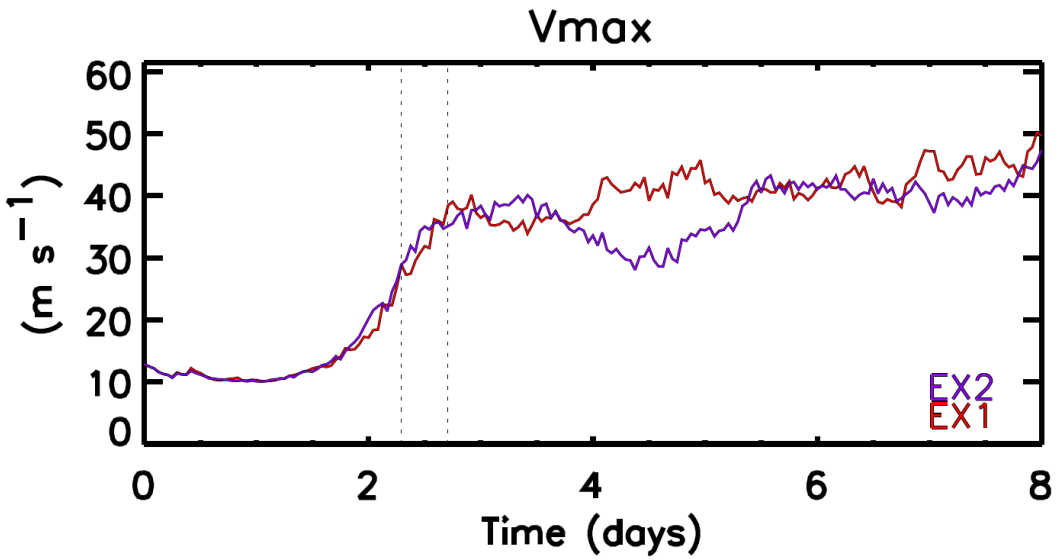

Summary Figure: Time-series of maximum azimuthally-averaged tangential wind **V**max for the two numerical experiments carried out in this study. The control experiment EX-1 (red) adopts the three-dimensional configuration used by Persing et al. (2013), but employs a uniform vertical grid spacing of 250 m in order to give increased vertical resolution in the upper tropospheric outflow region of the developing vortex. The suppressed vertical diffusivity experiment EX-2 (purple) is identical to EX-1 except that the vertical diffusivity Kv is set to zero everywhere above 1 km height. The results of these experiments demonstrate that the growth rates of EX-1 and EX-2 are essentially the same during the rapid intensification period (0 to 3 d). The analysis period 55 to 65 h discussed in detail in the study is shown by dotted lines.

On the hypothesized outflow control of tropical cyclone intensification

Michael T. Montgomery[a]*, John Persing[a], and Roger K. Smith[b]
[a] *Dept. of Meteorology, Naval Postgraduate School, Monterey, CA*
[b] *Meteorological Institute, Ludwig Maximilians University of Munich, Munich, Germany*
*Correspondence to: Prof. M. T. Montgomery, Naval Postgraduate School, 589 Dyer Rd., Root Hall, Monterey, CA 93943. E-mail: mtmontgo@nps.edu

We present idealized, three-dimensional, convection-permitting numerical experiments to evaluate the premise of the revised theory of tropical cyclone intensification proposed by Emanuel (2012). The premise is that small-scale turbulence in the upper tropospheric outflow layer determines the thermal stratification of the outflow and, in turn, an amplification of the system-scale tangential wind field above the boundary layer. The aim of our paper is to test whether parameterized small-scale turbulence in the outflow region of the developing storm is an essential process in the spin up of the maximum tangential winds.
Compared to the control experiment in which the small-scale, shear-stratified turbulence is parameterized in the usual way based on a Richardson number criterion, the vortex in a calculation without a parameterized representation of vertical mixing above the boundary layer has similar evolution of intensity. Richardson number near-criticality is found mainly in the upper-level outflow. However, the present solutions indicate that eddy processes in the eyewall play a significant role in determining the structure of moist entropy surfaces in the upper-level outflow. In the three-dimensional model, these eddy processes are largely realizations of asymmetric deep convection and are not obviously governed by any Richardson number-based criterion. The experiments do not support the premise on which the new theory is based. The results would appear to have ramifications for recent studies that invoke the new theory.

Key Words: Tropical cyclone, hurricane, typhoon, spin-up

Received December 17, 2018; Revised ; Accepted

Citation: . . .

1. Introduction

The steady-state hurricane model formulated by Emanuel (1986) has been a corner stone in underpinning the theory of hurricane behaviour for the last three decades. In particular, it has formed the basis for constructing a theory for the maximum Potential Intensity (PI) that a storm may achieve at a particular location. In PI theory, intensity is defined as the maximum gradient wind at the top of the frictional boundary layer. Over the years, the model has been refined in several ways (Emanuel 1988, 1995; Bister and Emanuel 1998) and it has been extended to provide a theory for storm intensification (Emanuel 1997, hereafter E97). An appraisal of the steady-state model and its application to PI theory is provided by Montgomery and Smith (2017, see section 5). An appraisal of the unsteady version of the model and its relation to other paradigms for hurricane intensification, including a new alternative rotating-convection paradigm, is given by Montgomery and Smith (2014).

The E97 intensification theory highlighted the fronto-genetic nature of eyewall formation, drawing upon the presumed (p. 1019) " ... crucial presence of downdrafts

by reducing the entropy tendency there (outside the radius of maximum tangential wind (RMW), our insertion) by a factor β". The factor β is assumed to be a function of radius. The key element of the time-dependent model was the derivation of an expression for the time rate-of-change of the tangential wind at the top of the boundary layer (his Eqn. [20]). This expression equates the tangential wind tendency to the sum of three terms. One of these terms is always negative definite, one vanishes at the radius of maximum gradient wind (RMW), and the third is positive only if the radial gradient of the '*ad hoc*' function, $\beta(r)$, is sufficiently negative to offset the other two terms. The function $\beta(r)$ is introduced to "... crudely represent the effects of convective and large-scale downdrafts, which import low θ_e ([equivalent potential temperature - our insertion) air into the subcloud layer" (p.1019, below Eqn. (16) of E97). One problem with the theory is the lack of a rigorous basis for the formulation of $\beta(r)$. A second problem is the assumption that the boundary layer is in approximate gradient wind balance. As discussed in Smith et al. (2008), this assumption is difficult to defend in the inner-core region of a tropical cyclone.

In a series of idealized, cloud-permitting numerical experiments, Montgomery et al. (2009) showed that tropical cyclone intensification does not require downdrafts, unlike the E97 theory. Further, they showed that vortex intensification proceeds optimally in the pseudo-adiabatic case in which downdrafts are excluded altogether. These results call into question the so-called β formulation of tropical cyclone intensification. They show also that the widely held Wind-Induced-Surface-Heat-Exchange (WISHE) evaporation-wind feedback mechanism of tropical cyclone intensification is neither essential nor the dominant pathway of intensification in the prototype problem for intensification (see Section 2a).

A few years ago, Emanuel and Rotunno (2011) and Emanuel (2012) questioned the assumption of Emanuel's earlier hurricane models (the steady model of Emanuel (1986) and the time-dependent E97 model) that the air parcels rising in the eyewall exit in the lower stratosphere in a region of approximately constant absolute temperature. To quote Emanuel (2012, p. 989): "Emanuel and Rotunno (2011) demonstrated that in numerically simulated tropical cyclones, the assumption of constant outflow temperature is poor and that, in the simulations, the outflow temperature increases rapidly with angular momentum." These authors proposed a revised theory[1] postulating that "the entropy stratification is determined by a requirement that the Richardson number not fall below a critical value" and that the temperature stratification of the outflow is determined by small-scale, shear-stratified turbulence.

Ordinarily, the critical Richardson number demarcates the local boundary between stratified shear stability and instability/turbulence[2]. Here it seems that small-scale turbulence in the outflow layer is presumed to operate and bound the Richardson number to a near critical value.

In the revised intensification theory of Emanuel (2012), small-scale, shear-stratified turbulence in the upper-tropospheric outflow layer is presumed to determine the thermal stratification of the upper-level outflow and, in turn, an amplification of the system-scale tangential wind field above the boundary layer. The new theory represents a major shift in the way a storm is presumed to be influenced by its environment. In the earlier models, it was assumed that the near-isothermal structure of the lower stratosphere set the (constant) outflow temperature. In the revised time-dependent theory, the vertical structure of the outflow temperature is determined internally within the vortex so that, in principal, it no longer matches the temperature structure of the storm environment. While the revised steady-state theory of Emanuel and Rotunno (2011) was configured to ensure that the outflow temperature at the radius of maximum wind (in angular momentum coordinates) equals the temperature of the environment (p2245)[3], the time-dependent theory does not appear to impose such a constraint.

A key result of the revised analytical intensification theory of Emanuel (2012) (see his section 3) is the derivation of a new expression for the time rate-of-change of tangential wind (his Eqn. [16]) (**?**, analogous to Eqn. [20)f]Emanuel1997. The right-hand side of this tendency equation involves three terms: the first term vanishes at the radius of maximum gradient wind; the third term is always negative definite and can only contribute to spin down; the second term is positive and must represent a generalized Coriolis force that depends on "the radial gradient of outflow temperature, which in turn, according to the results of Part I (Emanuel and Rotunno - our insertion), is a result of small-scale turbulence in the outflow region[4]."

On the face of it, the premise of the new intensification theory as articulated above appears implausible to us, at least from a fluid dynamics perspective, because of the tenuous link between small-scale mixing processes in the upper tropospheric outflow layer and the amplification of the system scale swirling wind at the top of the boundary layer. While the new theory makes numerous assumptions (some of which are highlighted later), to us the purported nature of this tangential force is the most mysterious facet of the revised theory. Another puzzling assumption used to generate solutions presented by Emanuel (2012), was the choice of an unrealistically large value of 5000 m for the boundary layer depth, h.

For the foregoing reasons an immediate question arises as to whether or not the premise of the new theory is physically defensible, at least for realistic parameter values

[1] In the revised theory, the maximum gradient wind is reduced by a factor of approximately $1/\sqrt{2}$ compared with the nominal potential intensity when the ratio of the bulk enthalpy exchange and drag coefficient is near unity ($C_k/C_D = 1$). The reduced intensity is a consequence of neglecting the pressure dependence of the saturation mixing ratio in the theory (see Emanuel and Rotunno 2011, pp. 2246-47).

[2] In fluid dynamics, a Richardson number of 0.25 defines the instability threshold for normal mode disturbances in the absence of moist processes (Drazin and Reid 1981). When turbulent processes are allowed for, the criticality boundary is usually extended to a value of unity based on simple energetics considerations (e.g., Cushman-Roisin 1994). In the revised steady state and intensification theories, this criticality boundary is tacitly assumed to hold true when moist processes are included.

[3] "... a shooting method is applied in which an outer radius [r_o - our insertion] is first specified, the system [defined by thier Equations (31) and (35) - our insertion] integrated, and the outflow temperature at the radius of maximum winds is noted. If it is not equal to T_t [the ambient tropopause temperature - our insertion], the integration is restarted with a new value of r_o, and so on, until the outflow temperature at the radius of maximum winds equals T_t".

[4] Later for pedagogical purposes we review in Appendix A the key assumptions and approximations underlying the new tendency equation and we derive the tendency equation from these assumptions. The derivation exposes *inter alia* the tangential force that is responsible for increasing the maximum tangential wind at the top of the boundary layer in the new theory.

consistent with the latest observational guidance? This question is relevant in view of recent studies that invoke the revised theory for the determination of a universal tangential wind profile for a hurricane (Chavas and Lin 2016) and as support for the integrity of a redefined Wind-Induced-Surface-Heat-Exchange (WISHE) intensification theory (Zhang and Emanuel 2016). The question is relevant also because the Emanuel (2012) theory has been invoked recently to suggest that tropical cyclones will be more prone to rapid intensification in a warmer climate, with the rate of storm intensification scaling as the square of the potential intensity (Emanuel 2017).

As an additional remark, it is worth pointing out that, because of the underlying axisymmetric formulation of the revised intensification theory, the hypothesis of small-scale, shear-stratified turbulence control on *vortex intensification* tacitly assumes that the shear stratified turbulence can be meaningfully represented as ring-like eddy structures encircling the vortex axis. In reality, such turbulent mixing occurs locally in azimuth and the axisymmetric assumption is highly questionable. Moreover, given the intrinsic limitations of vortex intensification in strict axisymmetric geometry in comparison with companion three-dimensional simulations (Persing et al. 2013), one should have a healthy skepticism for an axisymmetric theory of vortex spin up that invokes small-scale mixing processes in the upper troposphere to produce a generalized Coriolis force in the tangential direction to spin up the maximum tangential wind, which occurs at the top of the boundary layer. For these reasons, we will not use an axisymmetric model and use instead a three-dimensional model as the proper benchmark to evaluate the premise of the revised intensification theory.

We defer further discussion of the foregoing issues until later after we have summarized the results of two idealized, three-dimensional, experiments designed to test the new outflow control premise on vortex intensification for realistic parameter settings based on the latest observational guidance.

In the next section we describe the setup of the numerical experiments that are used to test the premise of the new intensification theory. The key results are discussed in Section 3 and a discussion of these and conclusions are the topic of Section 4.

2. The Model and Experiments

2.1. *Model core and pertinent parameter settings*

The model configuration relates to the prototype problem for tropical cyclone intensification. This problem considers the evolution of an initially cloud free, axisymmetric vortex of near tropical storm strength in thermal wind balance, embedded in a mean tropical environment without any ambient flow. The simulations are carried out using the numerical model of Bryan and Fritsch (2002), CM1 version 14. The reference sounding is the near-neutral sounding of Rotunno and Emanuel (1987). A detailed listing of the common and relevant numerical parameters and their definitions in the FORTRAN code is provided in Appendix B.

The simplest physics options are chosen to provide the cleanest possible comparison to the idealized framework of Emanuel (2012)'s new axisymmetric intensification theory. The effects of radiation are represented by Newtonian damping towards the reference sounding, with the damping rate capped at 2 K day^{-1}. The upper boundary includes a Rayleigh damping layer in the height range 20-25 km to control gravity wave noise reflected from the top boundary. Precipitation is represented by the simple scheme of Rotunno and Emanuel (1987) with a fixed fall speed for liquid water of 7 m s^{-1}. Ice microphysical processes are neglected. The foregoing options, while arguably difficult to justify for prolonged (multiple week) simulations (Persing et al. 2018), are adequate to simulate the intensification of an initial cyclonic vortex for the prototype problem on a realistic forecast time scale of order 5 days.

The calculations are carried out on an f-plane with the Coriolis parameter $f = 5 \times 10^{-5}$ s^{-1}, corresponding to 20°N. The sea surface temperature is fixed at 299.3 K (26.15 C).

2.2. *Sub grid-scale turbulence parameterization*

A bulk aerodynamic formulation for heat and enthalpy is used to model the turbulent momentum and enthalpy transfer at the sea surface and, for simplicity, the generally wind-speed dependent values of these exchange coefficients are taken to be constant. The enthalpy transfer coefficient is $C_k = 1.29 \times 10^{-3}$ and the drag coefficient is $C_{\rm D} = 2.58 \times 10^{-3}$. These constant values of surface exchange coefficients represent the best mean estimates from the latest in-situ observations under major hurricane conditions (Bell et al. 2012a).

The subgrid-scale turbulence is represented by choosing option "iturb=3" in the model, which is designed for problems that do not resolve any part of the turbulent Kolmogorov inertial range. This choice requires the specification of the horizontal mixing length $l_{\rm h} = 700$ m and the vertical mixing length $l_{\rm v} = 50$ m. These values are based on the recent observational findings of Zhang and Montgomery (2012) and Zhang et al. (2011b), respectively, and the resulting vertical and horizontal eddy diffusivities that are output in the model simulations. These values are also close to the values recommended by Bryan (2012) in order to produce realistic hurricane structure. For simplicity, these mixing lengths are assumed constant in both space and time.

The subgrid scale scheme follows the traditional formulation of Smagorinsky (1963) and Lilly (1962), except that different eddy viscosities are employed for the horizontal and vertical directions. As per the CM1 documentation, the flow-dependent momentum diffusivities in the horizontal and vertical directions are specified as follows: $K_{\rm m,h} = l_{\rm h}^2 S_{\rm h}$ and $K_{\rm m,v} = l_{\rm v}^2 S_{\rm v} \sqrt{1 - {\rm Ri}/{\rm Pr}}$, where the m subscript refers to momentum and the second subscript h or v refer to the horizontal and vertical directions, $S_{\rm h}$ and $S_{\rm v}$ denote the parts of the total deformation, S, that involve the horizontal and vertical strain components, ${\rm Ri} = N_m^2/S_{\rm v}^2$ is the moist Richardson number, N_m^2 is the moist Brunt-Väisälä frequency, and Pr is the Prandtl number (set to unity in this option) (see Bryan and Fritsch (2002) for complete definitions of these parameters). In this scheme, the heat and momentum diffusivities are taken to be identical, i.e. $K_{\rm h} = K_{\rm m}$ and the vertical eddy diffusivity is proportionally reduced in regions with positive moist Richardson number (< 1). Whenever Ri exceeds unity, $K_{\rm h,v}$ and $K_{\rm m,v}$ are set to zero.

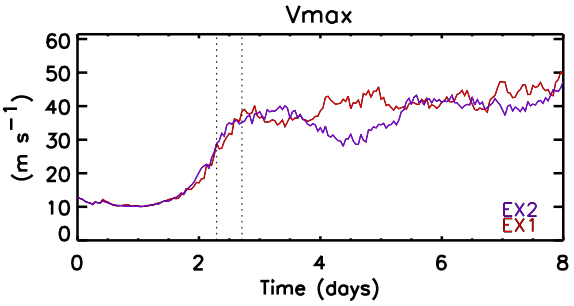

Figure 1. Time-series of maximum azimuthally-averaged tangential wind V_{max} for the control experiment EX-1 (red) and from the suppressed vertical diffusivity experiment EX-2 (blue) ($K_v = 0$ everywhere above 1 km height). The period 55 to 65 h is shown by dotted lines.

2.3. *Initial conditions*

The same initial cyclonic vortex is used for both simulations. The initial radial and vertical velocity are set to zero. The initial tangential velocity and temperature fields are in thermal wind balance (see appendix for further details). This tangential velocity has a maximum of 13 m s^{-1} at the surface at a radius of 100 km radius. It varies smoothly in space, declining to zero at a radius of 400 km radius, beyond which it is set to zero. It is set to zero also above a height of 20 km. Appendix B gives the mathematical formula for the tangential wind as per the CM1 model code and displays its radius-height structure.

2.4. *The experiments*

The control experiment, EX-1, is like the three-dimensional 3D3k simulation described by Persing et al. (2013) (with the same horizontal grid spacing described there, see Appendix B), except with a fixed vertical grid spacing of 250 m, so as to provide good resolution of the outflow layer (and a little better resolution than the 312.5 m grid spacing simulations employed by Emanuel and Rotunno (2011). Experiment EX-2 is similar to EX-1, but it is designed to suppress sub-grid scale mixing in the vertical direction above the boundary layer. Here, the vertical diffusivity K_v is set equal to zero at each time step above a height of 1 km. The suppression of vertical mixing by sub grid scale turbulence short circuits any presumed link between small-scale turbulence above the boundary layer and the amplification of tangential wind on the vortex scale. This remark applies, in particular, to parameterized small-scale turbulence in the upper-troposphere. If the new intensification theory of Emanuel (2012) is correct, then the vortex with zero vertical mixing should not intensify.

3. Results from idealized numerical experiments

3.1. *Vortex intensification compared*

Figure 1 shows a time series over an 8 day interval of the azimuthally-averaged maximum tangential velocity in the main experiments, EX-1 and EX-2. This time interval spans more than a typical forecast time scale of 3 to 5 days. The evolution of wind intensity until 90 hours is approximately the same in both simulations[5]. During this time the vortices intensify rapidly with a maximum spin up rate of around 1 m s^{-1} h^{-1} at 55 hours. After 72 h, barring fluctuations comparable in magnitude to the variability reported in Nguyen et al. (2008), the vortices continue to intensify with a reduced time-mean rate and achieve peak intensities of 50 m s^{-1} at 8 days.

3.2. *Outflow temperature evolution*

Figure 2 shows radius-time plots of the azimuthally-averaged temperature deviation from the environmental temperature near 11 km height in EX-1 and EX-2. The 11 km height is chosen because it corresponds approximately to the level where the Richardson number is most-frequently critical (see below). This height is where the shear-stratified (parameterized turbulent) mixing is hypothesized to have an important influence on the thermal and angular momentum structure of the vortex. The far-field environmental temperature at this altitude is 230.9 K, and remains near its initial value for the full simulation.

During the time interval covering the gestation and rapid intensification periods of the vortex (0 to 3 d), both experiments exhibit a progressively growing warm anomaly ($>$ 2K) inside a 50 km radius. Beyond this radius, the warm anomaly diminishes in strength until the 800 km radius where the outflow jet terminates (not shown). Emanuel's revised intensification theory presumes a modification of the thermal stratification of the air that emerges from the eyewall. In turn, this thermal structure controls the spin up of the vortex below. In EX-2, without vertical subgrid scale mixing, the evolution of the outflow temperature through rapid intensification (0 to 3 days) is very similar to that of EX-1. Beyond 3 days, the evolution of the outflow temperature exhibits more temporal fluctuation.

To investigate the possible dependence of the upper-tropospheric lapse rate on the parameterized vertical mixing, Figure 3 shows the deviation of the upper-level lapse rate from the environment for both the control (EX-1) and zero diffusivity experiment (EX-2). As above, the same height (11 km) is chosen for these lapse rate calculations. The lapse rate deviation within a radius of approximately 150 km shows a similar evolution for both experiments EX-1 and EX-2 through the bulk of the rapid intensification interval (0 to 2.5 days). After this time, the lapse rate deviation for EX-2 may be described as having somewhat more static stability than EX-1 at this height level between 100 and 1,000 km radius. At these longer times, specific events in EX-1 showing less static stability (more negative values in the figure) can be traced to outward propagating features that move with a radial speed of approximately 300 km day^{-1} (3.4 m s^{-1}). This diagnosis suggests that the radial structure of evolving lapse rate may be more-readily explained by outward advection of discrete features generated from the eyewall than a local subgrid scale mixing parameterization in the outflow region exterior to the eyewall.

In summary, the static stability in EX-2 is broadly similar to EX-1, but with generally greater stability. With static stability serving here as a proxy of $\partial s^{\star}/\partial M$, one must expect some difference in the simulated intensity of EX-2 relative to EX-1, but this is not found in Figure 1.

[5]For all of the experimental results presented here, the term 'intensity' is used in a more general sense than in PI theory and is defined as the azimuthally-averaged maximum tangential velocity. This maximum generally occurs in the frictional boundary layer at a height of approximately 600 m.

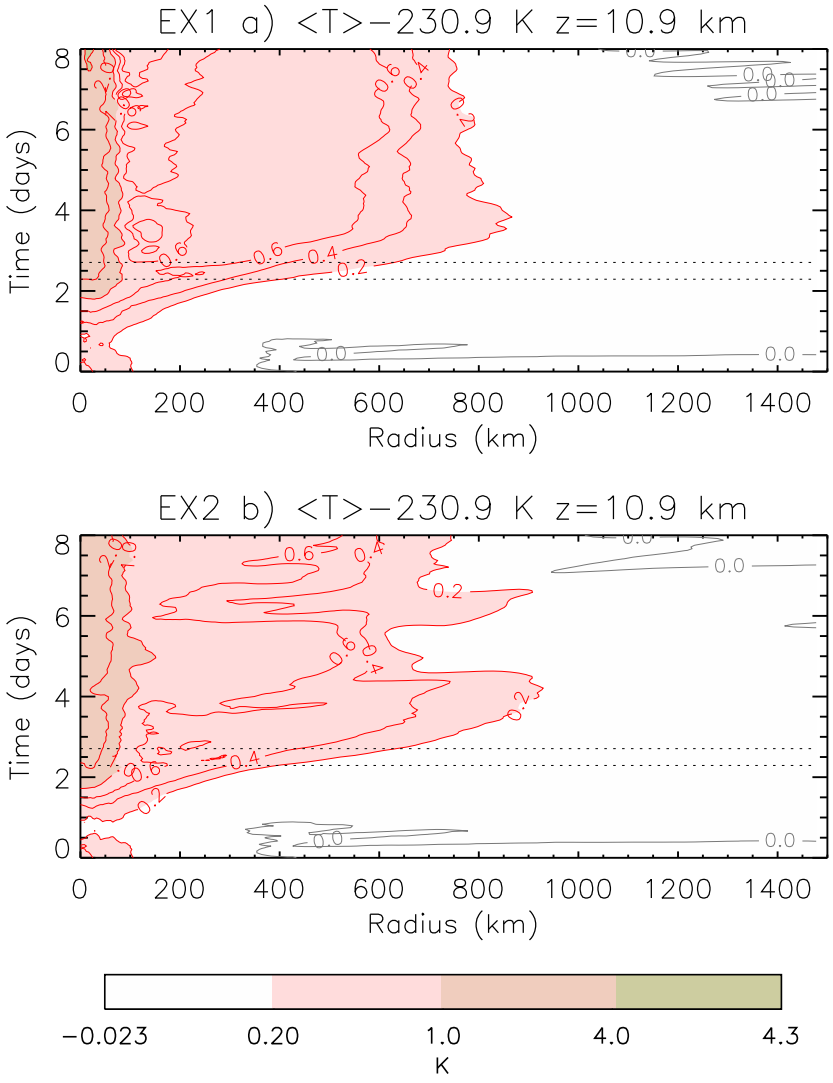

Figure 2. Radius-time contour plots of azimuthally-averaged temperature deviation from the far-field at 10.9 km height. The far-field temperature at this height is 230.9 K. Contours shown are $\pm\{0.2, 0.4, 0.6, 1.0, 2.0, 4.0\}$ K. Red contours denote positive values and blue contours denote negative values. Shading indicated in color bar. Top panel (a) for the control experiment EX-1, bottom panel (b) for experiment EX-2. The data shown are smoothed in time using a 5 hour boxcar smoother. The rapid intensification period spanning 55 to 65 h is highlighted by dotted lines.

3.3. *Richardson number structure*

In the CM1 model, the shear-stratified turbulence parameterization scheme is activated when the Richardson number has a value between zero and one. The gradient Richardson number in this model is implemented in Cartesian coordinates as follows

$$\mathrm{Ri}_{\mathrm{CM1}} = \frac{N_{\mathrm{m}}^2}{2\left(\frac{\partial w}{\partial z}\right)^2 + \left(\frac{\partial w}{\partial x} + \frac{\partial u_x}{\partial z}\right)^2 + \left(\frac{\partial w}{\partial y} + \frac{\partial u_y}{\partial z}\right)^2}, \quad (1)$$

with u_x, u_y, and w being the components of the wind in the x-, y-, and z-directions, respectively. Here, we evaluate this quantity in storm-centered cylindrical coordinates using

$$\mathrm{Ri}_{\mathrm{CM1}} = \frac{N_{\mathrm{m}}^2}{2\left(\frac{\partial w}{\partial z}\right)^2 + \left(\frac{1}{r}\frac{\partial w}{\partial \lambda} + \frac{\partial v}{\partial z}\right)^2 + \left(\frac{\partial w}{\partial r} + \frac{\partial u}{\partial z}\right)^2}, \quad (2)$$

where u, v, and w are the r-, λ-, and z-components of the velocity vector, respectively, and N_{m}^2 is the local moist static stability as computed by the numerical model (Durran and Klemp 1982). In the diagnosis presented here, the Richardson number is computed locally at every grid point on a (r, λ, z, t) grid, at one-hour intervals between 55 and 65 hours, during the rapid intensification phase (see Fig. 1)[6]. Figure 4 shows the azimuthal-time average of $\mathrm{Ri}_{\mathrm{CM1}}$ during this period for experiments EX-1 and EX-2. It shows also the relative frequency at which criticality (1.0 or below) occurs in each experiment at each (r, z) point within the 360 degree azimuth and during the 10 hour time averaging interval.

During the rapid intensification period in the control simulation, criticality is found (Fig. 4a) in the time-azimuth mean below the outflow around 11 km height and outside 60 km radius. A similar analysis for EX-2 (Fig. 4b) shows about the same extent of criticality. The low-level eyewall in both EX-1 and EX-2 has large spatial shears in the

[6]For the computation of $\mathrm{Ri}_{\mathrm{CM1}}$ shown here, the potential temperature, pressure, vapor and liquid mixing ratios, and tangential and radial wind components are interpolated to the cylindrical grid from the original Cartesian computational grid. The Richardson number is computed at each point on the cylindrical grid at each time, and then averaged.

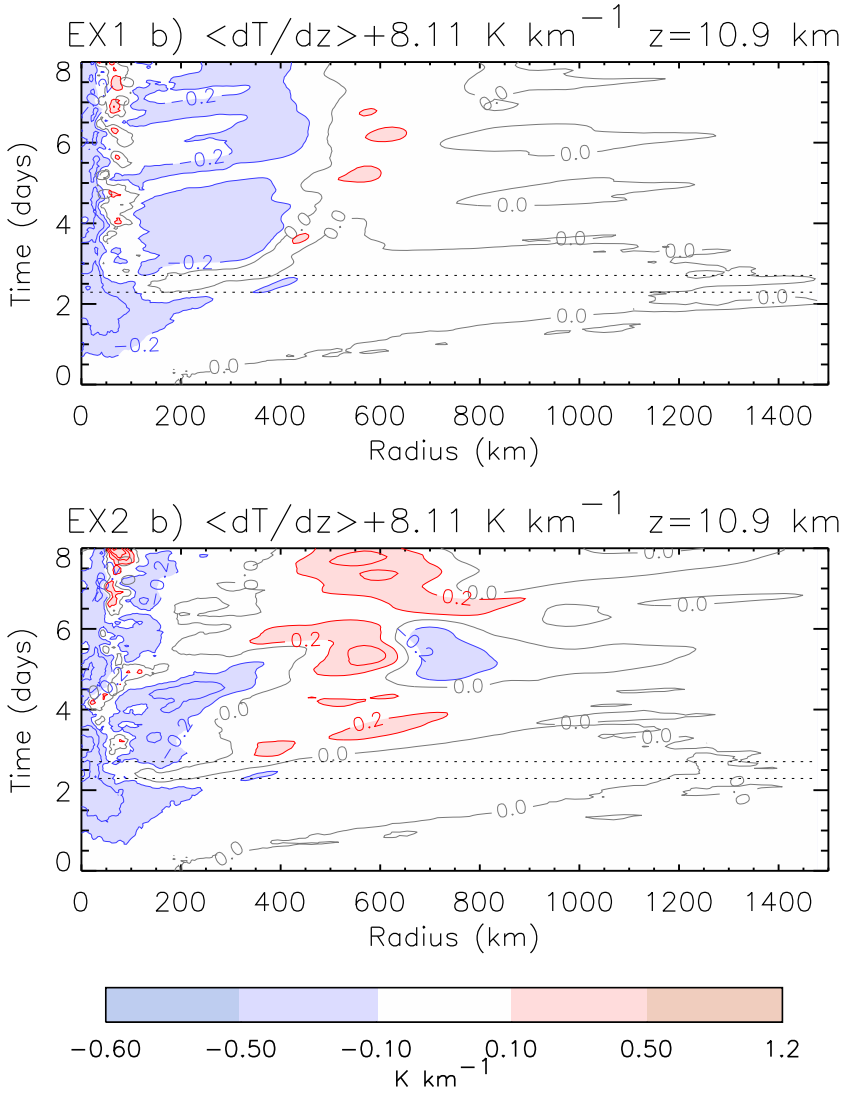

Figure 3. Radius-time contour plots of azimuthally-averaged lapse rate deviation from the far-field at 10.9 km height. The far-field lapse rate at this height is -8.11 K km^{-1}. Contours are shown with an interval of 0.1 K km^{-1}. Blue contours denote lapse rates that are greater (more negative) than the far-field and red contours denote lapse rates smaller (less negative) than the far-field. Shading indicated in the color bar. Top panel (a) for the control experiment EX-1, bottom panel (b) for experiment EX-2. The data shown are smoothed in time using a 5-hour boxcar smoother. The rapid intensification period spanning 55 to 65 h is highlighted by dotted lines.

flow, from which near-critical values of Richardson number are found extending up to 2 km height. The mid-level has relatively larger values of Richardson number. Frequencies of occurrence of criticality greater than 50% (red in Figs. 4c,d) are limited to the identified regions, above and below the upper-level outflow jet and in the low-level eyewall, plus a layer in middle of the planetary boundary layer at 500 m height.

3.4. Is there a relation between upper-level mixing and Richardson number?

Comparison of our computation of $\mathrm{Ri}_{\mathrm{CM1}}$ (Fig. 4a) with that of Figure 6a of Emanuel and Rotunno (2011) show a few differences which, for completeness, should be carefully considered. First, they display $\sqrt{\mathrm{Ri}}$. Second, they compute Richardson number based on the 24 hour averaged fields from an axisymmetric model versus our display of the time-azimuth average of Richardson number computed locally in space and time. Third, Emanuel and Rotunno (2011) display values from the mature stage, while we show values from the rapid intensifying stage (55-65 h). Our Figure 4a shows a region of criticality in the outflow region similar to that of Emanuel and Rotunno (2011) using the same metric[7]. We can confirm the large region of negative values of Ri through the mid-to-lower troposphere when we performed a separate computation with the Emanuel and Rotunno (2011) formula, hereafter $\mathrm{Ri}_{\mathrm{ER11}}$[8]. In the tropical atmosphere, one would expect to find a reversal of sign with height of $\partial s^*/\partial z$ (vertical gradient of saturated entropy, e.g. Holton 2004, Fig 11.1). The mean of $\mathrm{Ri}_{\mathrm{CM1}}$ does not show such a region of negative values through the mid-to-lower troposphere as does $\mathrm{Ri}_{\mathrm{ER11}}$. This difference is

[7]Our previous paper Persing et al. (2013) provided a preliminary analysis of the Richardson number in three-dimensional and axisymmetric hurricane simulations. We discovered a coding error in our previous diagnosis of the gradient Richardson number that over-reported the value of this number. This error has been corrected here.

[8]We presume that Emanuel and Rotunno (2011) also computed negative values of $\mathrm{Ri}_{\mathrm{ER11}}$, and that as an expedient they have displayed imaginary values of $\sqrt{\mathrm{Ri}_{\mathrm{ER11}}}$ as zero.

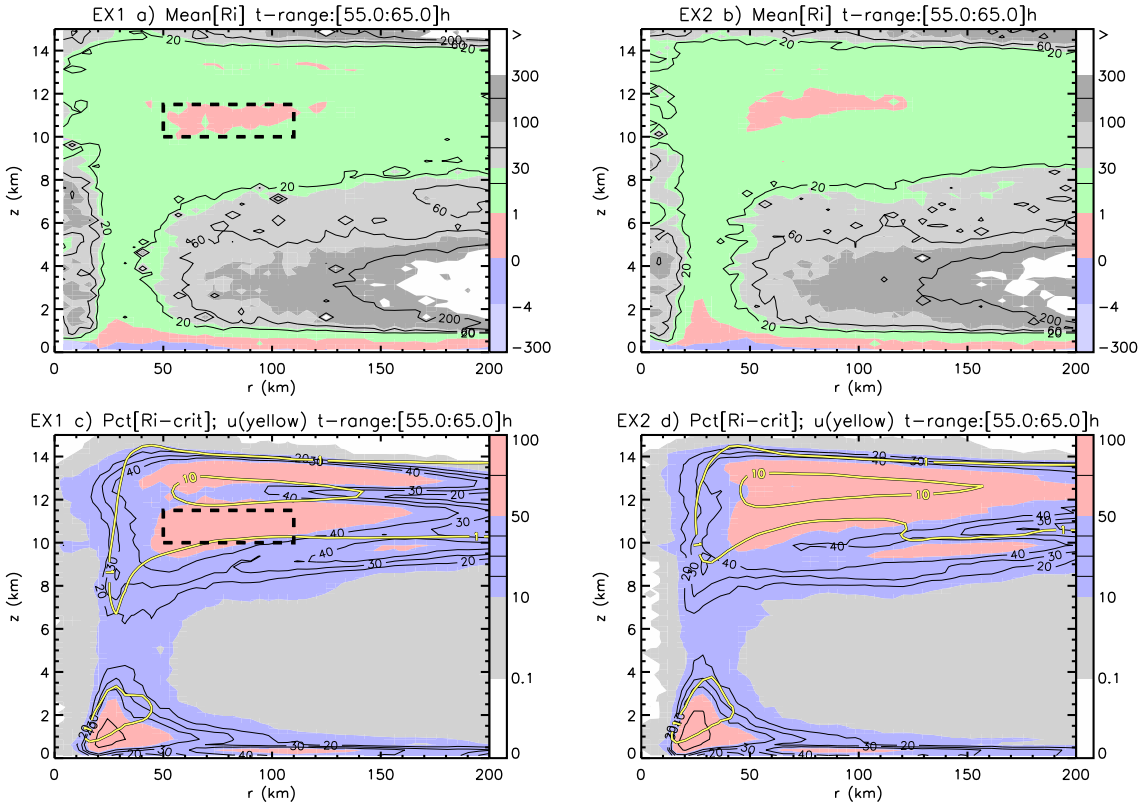

Figure 4. Panels (a) and (b) show radius-height structure of azimuthal-time-mean gradient Richardson number $\mathrm{Ri}_{\mathrm{CM1}}$ for experiments EX-1 and EX-2, respectively. Values are shown by shading indicated in the color bar. Supplemental contours of 20, 60, and 200 are shown also. Panels (c) and (d) show the relative frequency ('PCT') of occurrence of $0 \leq \mathrm{Ri}_{\mathrm{CM1}} \leq 1$ (marking criticality) at each (r, z) coordinate during the time intervals $55 \leq t \leq 65$ h. Frequency is shown by shading indicated in the color bar. Supplemental contours of 20, 30, 40, and 75 % are shown also. The azimuthal-time mean outflow jet is indicated by the yellow curves in panels (c) and (d) with contours of 1 and 10 m s^{-1}. The dashed box denotes an annulus of criticality referred to in the text.

attributable in part to how the CM1 model uses a separate dry calculation for uncloudy grid cells and to the somewhat different formulation of N_m^2 in the cloudy cells. Where the water vapor content is small in the upper troposphere, the CM1 formulation (based on Durran and Klemp (1982)) and Emanuel and Rotunno (2011) formulation should (and do) agree.

In CM1, by design, the quantity $\mathrm{Ri}_{\mathrm{CM1}}$ controls the activation of a sub-grid scale vertical mixing parameterization when $\mathrm{Ri}_{\mathrm{CM1}} < 1$, thereby initiating subgrid scale mixing associated with shear-stratified turbulence. Activation of shear-stratified turbulence is prevalent in the outflow of EX1, but in EX2, where this process is artificially suppressed, there is essentially no significant difference in evolution of intensity from EX-1 during the main intensification period. The EX2 simulation shows greater spatio-temporal variability of the secondary circulation and in turn a more extensive region of criticality than EX1 (Fig. 4d), even as the spatio-temporal averaged $\mathrm{Ri}_{\mathrm{CM1}}$ is very similar in the outflow (Fig. 4a,b). We conclude that mixing by shear-stratified turbulence is not essential for tropical cyclone intensification in the prototype problem using standard values of the model parameters and using the latest observational guidance for horizontal and vertical turbulence mixing lengths in real tropical cyclones.

The question remains as to what degree the postulated shear-stratified turbulent signature is identifiable in the simulated CM1 data? The revised PI theory of Emanuel and Rotunno (2011) presumes subgrid scale mixing of entropy across M-surfaces to determine the outflow stratification. To examine this question, we use equivalent potential temperature θ_e as a proxy for moist entropy. Figure 5 quantifies the eddy and diffusive fluxes of θ_e that contribute to the redistribution of θ_e across M-surfaces in EX-1 for the same time period as Figure 4. All quantities plotted in this figure are time averaged over the time interval $55 \leq t \leq 65$ h for experiment EX-1 and averaged azimuthally also. Two challenges that arise in applying the Emanuel and Rotunno (2011) theory should be noted here. First, the core of the outflow jet (Fig. 5a), presumably originating from the strongest updrafts found near the radius of maximum winds, is a region of large values of Richardson number (values up to 20 in Fig. 4a), thus spoiling a basic tenet of Emanuel and Rotunno (2011). Second, the explicit assumption in Emanuel and Rotunno (2011) (p. 2243) that there is a one-to-one relationship between M and saturation entropy is violated in the simulation by the folding of the M-surfaces at various levels of the outflow jet (Fig. 5c,d).

As evident in Figure 4, there is an annulus of criticality where $\mathrm{Ri}_{\mathrm{CM1}}$ is predominantly less than one ($50 \leq r \leq 110$ km, $10 \leq z \leq 11.5$ km). Accordingly, in this region one would expect to find some footprint of the proposed mixing process. In Figure 4c, we see that this annulus is located in the outflow jet below the jet maximum. The two principal signals of entropy mixing are the resolved radial (Figure 5e) and resolved vertical (Figure 5f) eddy fluxes of θ_e. The corresponding diffusive flux terms (Figures 5g and 5h) are found to be at least an order of magnitude smaller (note the smaller contour values of panels g and h). The resolved eddy fluxes are largest near the eyewall and are of

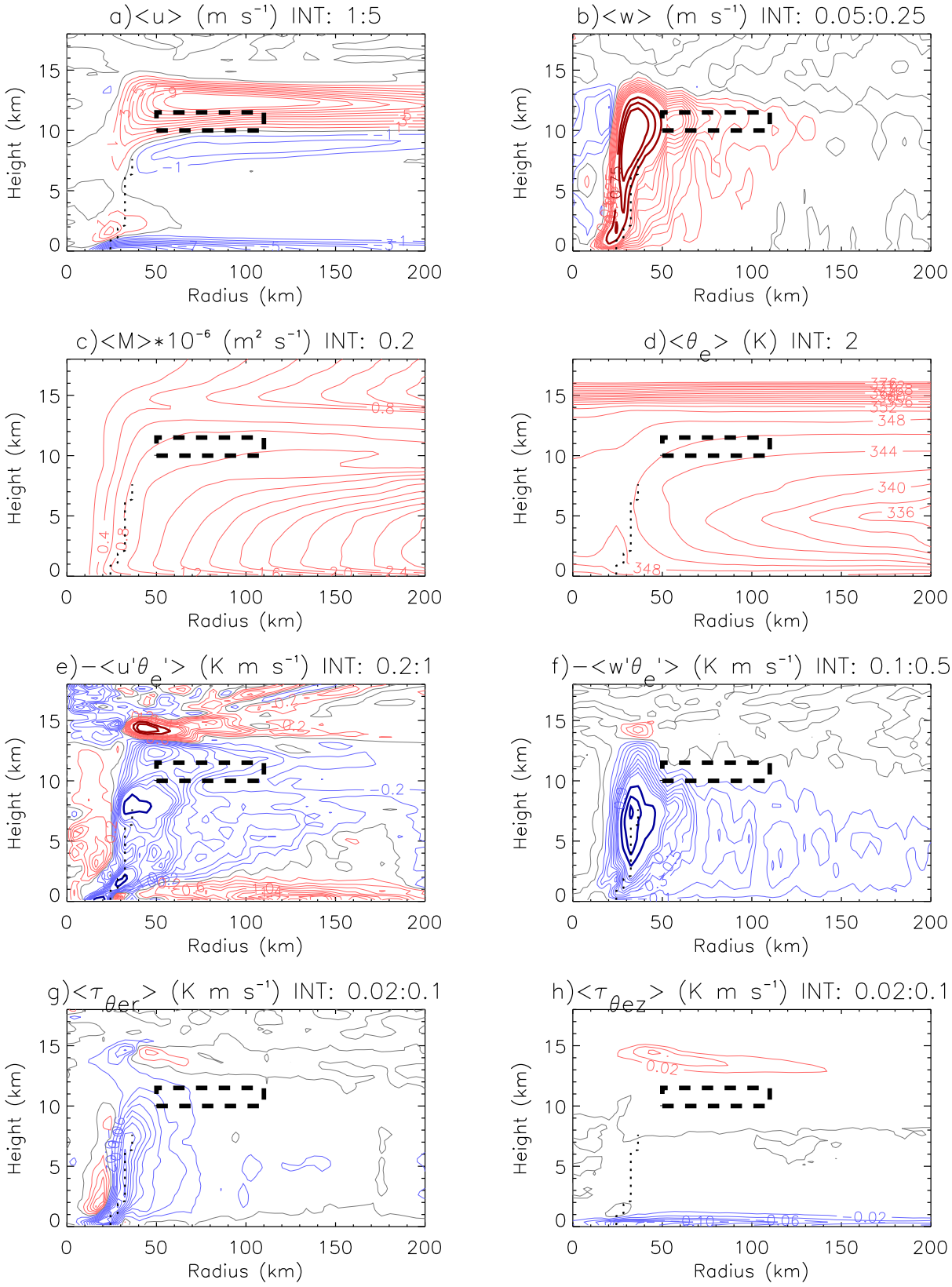

Figure 5. Contours of azimuthal-time-mean quantities (indicated by a bracket symbol) from EX-1 for a time period during vortex intensification, 55 to 65 h, plotted as a function of radius and height, with positive contours red, zero contour in grey, and negative contours in blue. The dotted curve shows the radius of the maximum azimuthally-averaged tangential wind as a function of height below 7 km height. (a) mean radial wind $\langle u \rangle$ with contour interval of 1 m s^{-1}. (b) mean vertical velocity $\langle w \rangle$ with contour interval of 0.05 m s^{-1} (thin) and 0.25 m s^{-1} (thick) beginning at 0.75 m s^{-1}. (c) mean absolute angular momentum $\langle M \rangle$, shown with values divided by 10^6, with contour interval of 0.2 m^2 s^{-1}. d) mean equivalent potential temperature $\langle \theta_e \rangle$ with contour interval of 5 K. (e) $-\langle u'\theta_e' \rangle$, the mean radial eddy flux of θ_e, with contour interval 0.2 K m s^{-1} (thin) and 1 K m s^{-1} (thick) starting at $\pm$3 K m s^{-1}. (f) $-\langle w'\theta_e' \rangle$, the mean vertical eddy flux of θ_e, with contour interval 0.1 K m s^{-1} (thin) and 0.5 K m s^{-1} (thick) starting at $\pm$1.5 K m s^{-1}. (g) $\langle \tau_{\theta_e r} \rangle$, the parameterized mean radial flux of θ_e corresponding to (e) with contour interval 0.02 K m s^{-1}. (h) $\langle \tau_{\theta_e z} \rangle$, the parameterized mean vertical flux of θ_e corresponding to (f) with contour interval 0.02 K m s^{-1}. The black dotted box is the same as that shown in Figure 4.

lesser magnitude in the upper-level outflow. Of interest also is that the Richardson-number based mixing represented by $\tau_{\theta_e z}$ shows contours above the core of the outflow jet and not in the annulus highlighted by the box; this region above the core of the outflow shows θ_e-contours connected with the stratosphere and unconnected with the planetary boundary layer. Based on these results, it would seem highly implausible that this region of subgrid scale mixing could contribute to the spin up of the vortex at the top of the boundary layer as presumed in Emanuel (2012).

On the basis of the foregoing evidence, it would seem that the rearrangement of entropy occurs mainly in the eyewall region. Moreover, Ri-criticality, which is limited to the outflow, bears little relation to this rearrangement process. The identified eddy processes in the eyewall are largely realizations of asymmetric deep convection in the model and are not obviously governed by any Richardson number-based criterion.

4. Discussion and conclusions

We have used two idealized, three-dimensional, numerical experiments to evaluate the premise of the revised theory of tropical cyclone intensification proposed by Emanuel (2012). In the revised theory, small-scale turbulence in the upper tropospheric outflow layer is hypothesized to determine the distribution of moist entropy and thermal stratification of the outflow and, in turn, *an amplification of the system-scale tangential wind field above the boundary layer*.

As noted in the Introduction, there are intrinsic differences between the behaviour of tropical cyclone vortices in axisymmetric and three-dimensional configurations (e.g. Persing et al. 2013). Since small-scale, shear-stratified turbulence is a local phenomenon and one that is not well approximated by axisymmetric rings, one should be cautiously skeptical of results from axisymmetric simulations that project this process into axisymmetric rings. The three dimensional model should be regarded as the proper benchmark.

Compared to the control experiment in which the small-scale, shear-stratified turbulence is parameterized in the usual way based on a standard Richardson number criterion, the vortex in a calculation without any representation of vertical diffusion above the boundary layer evolves in a similar way with no significant difference in the intensification rate of the maximum azimuthally-averaged tangential velocity, upper-level outflow temperature, or outflow thermal stratification.

Despite the statement of Emanuel (2012) that "... the critical Richardson number hypothesis leads to predictions of storm evolution that are also, for the most part, in good accord with (axisymmetric, our insertion) numerical simulations", our three-dimensional calculations using plausibly realistic values of the subgrid-scale turbulence parameters do not support the revised theory. Indeed, they cast strong doubt on the premise of this theory that small-scale, shear-stratified turbulence in the upper-level outflow of the developing vortex controls the intensification of the vortex. Even if the upper-tropospheric mixing leads to a generalized Coriolis force at the top of the layer with friction, which is shown in the Appendix to be at the heart of the revised intensification theory, it does not appear to manifest itself in the control experiment for realistic subgrid scale parameters.

We have offered an explanation for the different conclusions from the different numerical models and Richardson number closure formulations used by Emanuel (2012) and the present study. For the three-dimensional experiment with parameterized mixing, the rearrangement of moist entropy is found to occur mainly in the eyewall region. The diagnosed eddy processes in the eyewall are largely realizations of asymmetric deep convection in the model and are not obviously governed by any Richardson number-based criterion.

These findings are believed to be significant in the light of recent studies that invoke the revised theory for the determination of a universal tangential wind profile in hurricanes and as support for the integrity of a redefined Wind-Induced-Surface-Heat-Exchange (WISHE) intensification theory.

Acknowledgements

MTM and JP acknowledge the support of NSF grant AGS-1313948, NOAA HFIP grant N0017315WR00048, NASA grant NNG11PK021, ONR grant N0001417WX00336, and the U. S. Naval Postgraduate School. RKS acknowledges financial support from the German Research Council (Grant SM30-23) and the Office of Naval Research Global (Grant N62909-15-1-N021). The views expressed herein are those of the authors and do not represent sponsoring agencies or institutions. The data used in this paper can be accessed by emailing the first author at: mtmontgo@nps.edu.

Appendix A: Derivation of revised tendency equation and azimuthal force

Here we review the key approximations and assumptions underpinning the tendency equation of Emanuel (2012, hereafter E12), the revised intensification theory. In particular, we derive the tendency equation from the stated assumptions[9]. The derivation exposes the tangential force that is responsible for amplifying the maximum tangential wind at the top of the boundary layer in the new axisymmetric theory. Amidst the derivation, some additional questions arise about the theory and its proffered analytical solution.

The starting point of the revised theory is the axisymmetric equation for the depth-averaged boundary layer moist entropy s_b in absolute angular momentum ($M = rv + 1/2fr^2$) and pressure coordinates (Eq. (12) in E12):

$$h\frac{\partial s_b}{\partial \tau} - C_{\rm D} r|\mathbf{V}|V\frac{\partial s_b}{\partial M} = C_k|\mathbf{V}|(s_0^* - s_b) + C_{\rm D}\frac{|\mathbf{V}|^3}{T_s}, \tag{3}$$

where $C_{\rm D}$ and C_k are the surface exchange coefficients for momentum and enthalpy, $\mathbf{V}$ is the Reynolds-averaged velocity vector averaged across the boundary layer, s_0^* is the saturation moist entropy (defined below) at the sea surface

[9] Although we accept here the basic assumptions of the E12 theory for the purposes of gaining basic understanding, this should not be interpreted as our endorsement of these assumptions when applied to real or simulated storms in a three-dimensional configuration. In particular, we would step back from endorsing the assumption of axisymmetric moist neutral flow on the grounds that intensification is intrinsically non-axisymmetric and that M and θ_e surfaces only approach a state of congruence *after* the intensification process is already well under way (Kilroy, personnal communication).

temperature, T_s, and h is the boundary layer depth, assumed to be constant. Here τ is the dimensional time variable wherein partial derivatives with respect to τ hold M and p constant. The boundary layer depth $h = \Delta p_b/\rho g$, where Δp_b is the boundary layer depth (in pressure units), ρ is the density averaged over the boundary layer and g is the gravitational acceleration.

The two terms on the left hand side of the entropy equation are the local time tendency of s_b and the depth-averaged radial advection of s_b in M-coordinates. (The latter uses the fact that in M-coordinates the radial velocity u_M is defined by $u_M = DM/Dt$ and $hDM/Dt = -C_{\rm D} r|\mathbf{V}|V$ from the angular momentum equation integrated over the boundary layer). The right hand side of the entropy equation consists, respectively, of the bulk-aerodynamic parameterization of the vertical transfer of moist entropy between the underlying ocean and the moist air at anemometer level and a bulk representation of dissipative heating (and corresponding entropy production). By definition, radial and vertical eddy entropy and angular momentum fluxes are zero in the axisymmetric theory.

The saturation moist entropy is given by

$$s^* = c_p \ln T - R_d \ln p + \frac{L_v q_v^*}{T} \tag{4}$$

where c_p is the specific heat of dry air at constant pressure, T is the temperature, R_d is the gas constant of dry air, p is the pressure, q_v^* is the saturation water vapour mixing ratio, and L_v is the latent heat of condensation.

The quantity s_0^* denotes the saturation entropy at the sea surface temperature

$$s_0^* = c_p \ln T_s - R_d \ln p_0 + \frac{L_v q_{v0}^*}{T_s} \tag{5}$$

where p_0 is the surface pressure and q_{v0}^* is the surface saturated vapor mixing ratio. It will prove useful later to note that if we neglect the pressure dependence of s_0^* and use the environment values to evaluate this quantity, then the M derivative of s_0^* will vanish (see below for more).

The three principal approximations that are invoked to derive the tendency equation in the new theory are the following:

- (a) neglect the pressure dependence of s_0^*;
- (b) neglect dissipative heating;
- (c) approximate $|\mathbf{V}|$ and V by V_g

where V_g is the gradient wind.

In the eyewall region, moist air rises out of the boundary layer, rapidly condenses, and ascends in cloud along M surfaces (slantwise convective neutrality). Thus, along an M surface, the saturated entropy above the boundary layer is assumed equal to the originating boundary layer entropy, $s^* = s_b$, whereupon

$$V^2 = -(T_b - T_o) M \frac{\partial s^*}{\partial M}, \tag{6}$$

where T_b is the boundary layer temperature and T_o is the outflow temperature. This equation is a form of the thermal wind equation. The variation of the outflow temperature with M is then assumed to be controlled by the action of shear-stratified turbulence wherein the gradient Richardson number is bound to a near critical value

$$\frac{\partial T_o}{\partial M} = -\frac{{\rm Ri}_c}{r_t^2}\left(\frac{\partial s^*}{\partial M}\right)^{-1} \tag{7}$$

which is a turbulence closure assumption on the outflow. In this equation r_t denotes the radius where the gradient Richardson number first becomes critical in the outflow layer.

The moist entropy equation at the top of the boundary layer is then

$$h\frac{\partial s^*}{\partial \tau} - C_{\rm D} V M \frac{\partial s^*}{\partial M} = C_k V (s_0^* - s^*) \tag{8}$$

Now $\frac{\partial}{\partial M}$ of Eq. (8) gives

$$h\frac{\partial}{\partial \tau}\frac{\partial s^*}{\partial M} - C_{\rm D}\frac{\partial}{\partial M}\left(VM\frac{\partial s^*}{\partial M}\right) = C_k \frac{\partial}{\partial M}[V(s_0^* - s^*)] \tag{9}$$

but Eq. (6) gives

$$\frac{\partial s^*}{\partial M} = \frac{-V^2}{(T_b - T_o)}\frac{1}{M}$$

whereupon, the first term on the left hand side of Eq. (9) becomes[10]

$$-\frac{h}{M}\frac{\partial}{\partial \tau}\left(\frac{V^2}{T_b - T_o}\right) \tag{10}$$

and the second term on the left hand side becomes

$$\begin{aligned} &- C_{\rm D}\frac{\partial}{\partial M}\left(VM\frac{\partial s^*}{\partial M}\right) \\ &= C_{\rm D}\frac{\partial}{\partial M}\left(\frac{V^3}{T_b - T_o}\right) \\ &= \frac{3C_{\rm D}V^2}{T_b - T_o}\frac{\partial V}{\partial M} + C_{\rm D}V^3\frac{\partial}{\partial M}\left(\frac{1}{T_b - T_o}\right). \end{aligned} \tag{11}$$

Now E12 makes the additional approximation

$$\frac{\partial}{\partial M}\left(\frac{1}{T_b - T_o}\right) \approx \frac{1}{(T_b - T_o)^2}\frac{\partial T_o}{\partial M}$$

This approximation follows from the assumption that T_b, the temperature after integrating across the boundary layer, is assumed to be a constant in radius (and hence M).

At this point the turbulence closure assumption, Eq. (7), is applied and $\partial s^*/\partial M$ is substituted using Eq. (6) so that

$$\begin{aligned} \frac{\partial}{\partial M}\left(\frac{1}{T_b - T_o}\right) &= \frac{-1}{(T_b - T_o)^2}\frac{{\rm Ri}_c}{r_t^2}\left(\frac{\partial s^*}{\partial M}\right)^{-1} \\ &= \frac{-1}{(T_b - T_o)^2}\frac{{\rm Ri}_c}{r_t^2} \times -\frac{M(T_b - T_o)}{V^2} \\ &= \frac{M}{V^2(T_b - T_o)}\frac{{\rm Ri}_c}{r_t^2} \end{aligned} \tag{12}$$

The term on the right of Eq. (9) becomes

$$\begin{aligned} &C_k\frac{\partial}{\partial M}[V(s_0^* - s^*)] \\ &\quad = C_k(s_0^* - s^*)\frac{\partial V}{\partial M} + C_k V\frac{\partial}{\partial M}(s_0^* - s^*) \end{aligned} \tag{13}$$

[10] Note that M is an independent variable so that $\partial M/\partial \tau = 0$.

and E12 writes the second term on the right hand side of this equation as

$$C_k V \frac{\partial}{\partial M}(s_0^* - s^*) \approx -C_k V \frac{\partial s^*}{\partial M} = \frac{C_k V^3}{M(T_b - T_o)}, \quad (14)$$

using Eq. (6) and neglecting the pressure dependence of s_0^* (as foreshadowed above).

Collecting the terms in Eq. (9) together now gives (using (10) - (14)),

$$\begin{aligned} -\frac{h}{M}\frac{\partial}{\partial \tau}\left(\frac{V^2}{T_b - T_o}\right) = &-\frac{3C_D V^2}{T_b - T_o}\frac{\partial V}{\partial M} \\ &- \frac{C_D V M}{(T_b - T_o)}\frac{\mathrm{Ri}_c}{r_t^2} \\ &+ C_k(s_0^* - s^*)\frac{\partial V}{\partial M} \\ &+ \frac{C_k V^3}{M(T_b - T_o)} \end{aligned} \quad (15)$$

or, cleaning up,

$$\begin{aligned} \frac{h}{M}\frac{\partial}{\partial \tau}\left(\frac{V^2}{T_b - T_o}\right) = &\frac{\partial V}{\partial M}\left[\frac{3C_D V^2}{T_b - T_o} - C_k(s_0^* - s^*)\right] \\ &+ \frac{C_D V M}{(T_b - T_o)}\frac{\mathrm{Ri}_c}{r_t^2} - \frac{C_k V^3}{M(T_b - T_o)} \end{aligned} \quad (16)$$

Multiplying the last equation by $M(T_b - T_o)/(hV)$ gives Eq. (16) of E12:

$$\begin{aligned} &\frac{T_b - T_o}{V}\frac{\partial}{\partial \tau}\left(\frac{V^2}{T_b - T_o}\right) \\ &= \frac{M}{hV}\frac{\partial V}{\partial M}\left[3C_D V^2 - C_k(T_b - T_o)(s_0^* - s^*)\right] \\ &+ \frac{C_D}{h}\frac{\mathrm{Ri}_c}{r_t^2}M^2 - \frac{C_k}{h}V^2 \end{aligned} \quad (17)$$

At V_m (the maximum tangential wind), $\partial V/\partial M = 0$, whereupon Eq. (17) simplifies to

$$\frac{T_b - T_o}{V}\frac{\partial}{\partial \tau}\left(\frac{V^2}{T_b - T_o}\right) = \frac{C_D}{h}\frac{\mathrm{Ri}_c}{r_t^2}M^2 - \frac{C_k}{h}V^2. \quad (18)$$

E12 (p. 992) assumes that the outflow temperature at the RMW equals the tropopause temperature, i.e., $T_o = T_t$, with the latter assumed constant in time. This implies that the time derivative of T_o vanishes at the RMW. We can thus simplify the time derivative in the foregoing equation to obtain the tangential velocity tendency equation at the RMW:

$$\frac{\partial V_m}{\partial \tau} = \underbrace{\frac{C_D}{2h}\frac{\mathrm{Ri}_c}{r_t^2}M^2}_{>0} - \underbrace{\frac{C_k}{2h}V_m^2}_{>0}, \quad (19)$$

where V_m denotes the maximum tangential velocity at the top of the boundary layer.

The foregoing is a tendency equation for V_m forced by two terms on the right hand side. The first term is positive and denotes the tangential (generalized Coriolis) force per unit mass that increases V_m with time. This term is proportional to the drag coefficient and the critical gradient Richardson number. The second term is negative and arises in association with the depletion of tangential momentum in the boundary layer. Curiously, however, this second term is proportional to the enthalpy transfer coefficient C_k. One would ordinarily expect this term to be proportional to the drag coefficient C_D. E12 notes however that the equation is not yet closed and argues that it is possible that the global solution dependence on C_k may be different than would be apparent solely from an examination of this term at this stage in the derivation.

E12 proceeds to make an additional (and, in our view, unsubstantiated) assumption that the RMW always lies on the same M surface. Combining this assumption with an algebraic relation deduced from the revised steady-state theory (not written here), E12 derives an analytical (closed-form) solution for the evolution of V_m (his Eq. (19))[11]. The novelty of the result notwithstanding, the apparent elegance of the analytical solution conceals the essential role of the azimuthal force in amplifying V_m.

The critical role of the tangential force may be exposed by repeating the foregoing derivation while discarding the closure equation for the outflow temperature. In this case, one obtains at the RMW

$$\frac{\partial V_m}{\partial \tau} = \frac{C_D {V_m}^2 M}{2h(T_b - T_t)}\frac{\partial T_o}{\partial M} - \frac{C_k}{2h}V_m^2, \quad (20)$$

where T_t denotes the tropopause temperature at the RMW (assumed equal to T_o and independent of time). While other outflow closures are conceivable that would, in turn, change the specification of $\partial T_o/\partial M$, if one employs the traditional Emanuel formulation of a constant outflow temperature (e.g. E97 with $\beta = 0$), then $\partial T_o/\partial M$ would be identically zero. The resulting tendency equation for V_m in this case consists only of the second term on the right hand side of Equation (20), which is negative definite. Thus without the force in the traditional formulation of the upper boundary condition, the vortex spins down! Notwithstanding this fact, we have a more fundamental issue with the physics encompassed by Equation (20). We find it puzzling how, in reality, the stratification of the outflow layer ($\partial T_o/\partial M$) would act to move the M surfaces inwards in a way to amplify the tangential wind at the top of the boundary layer. A similar remark would apply to Equation (19), in which $\partial T_o/\partial M$ has a specific parameterization.

Appendix B: Model parameters used in numerical experiments

This appendix documents the common numerical parameters used in the numerical experiments presented in this study and those parameters that relate to specific decisions made in specifying the EX-1 simulation. Although there is some repetition of material with that of

[11] The closed-form solution strictly applies only for the case in which the initial tangential velocity is everywhere zero.

Section 2, we list all of the pertinent model parameters for completeness. This documentation would allow the reader to download the numerical model and repeat the experiments presented herein. The numerical model, CM1, is publicly available at George Bryan's UCAR webpage (www2.mmm.ucar.edu/people/bryan). Version 14 (CM1v14) is used in this study; most of these parameters are common to later versions of CM1, others though are no longer supported. A name list file is used to set many parameters of the simulation at the time of execution. Simulations were performed on a Red Hat Linux cluster, kernel release 2.6.32-358.13.1.e16.x86_64 dated 17 June 2013 for x86_64 architecture using the Portland Group compiler with NetCDF support.

The grid mesh is a stretched grid in the horizontal with origin at the center of the domain (*iorigin=2*). In the middle of the domain in the horizontal is a fine-mesh grid region 405 $\times$ 405 km square with fixed grid spacing of 3 km in both the x- and y-directions. The grid configuration is established in the name list file with 185 grid points in the x- and y- directions (*nx=185, ny=185*) with stretching (*stretch_x=1, stretch_y=1*), an inner grid spacing of 3 km (*dx_inner=3000.0, dy_inner=3000.0*), an outer grid spacing of 100 km (*dx_outer=100000.0, dy_outer=100000.0*), a no-stretch length of 405 km (centered on the origin at the middle of the domain) (*nos_x_len=405000.0, nos_y_len=405000.0*), and total domain size of 2980 $\times$ 2980 km (*tot_x_len=2980000.0, tot_y_len=2980000.0*).

The vertical grid mesh has 100 points (*nz=100*) on a mesh with fixed grid spacing (*stretch_z=0, dz=250.0*)).

The equations of Bryan and Fritsch (2002) with a Runge-Kutta integrator with condensation adjustment is used (*neweqts=2*). The horizontal and vertical advection use a 5th-order scheme (*hadvorder=5, vadvorder=5*) and diffusion uses the recommended 6th-order scheme with diffusion coefficient 0.04 (*difforder=6, kdiff6=0.040*) which is in addition to the parameterized turbulence below. A vertically implicit Klemp and Wilhelmson (1978) time-splitting is used for acoustic modes (*psolver=3*), with six small time steps for each large time step (*nsound=6*). The vertically-implicit acoustic solver uses an off-centering coefficient of 0.60, which is slightly forward in time (*alph=0.60*). Potential temperature is not integrated on the small time steps (*thsmall=0*). The coefficient for a divergence damper is 0.1 (*kdiv=0.10*). As discussed in section 2, parameterized turbulence is used (*iturb=3*) with vertical and horizontal mixing length scales $l_v = 50$ m and $l_h = 700$ m (*l_v=50.0, l_h=700.0*) based on the recent observational findings of Zhang et al. (2011a) and Zhang and Montgomery (2012), and the resulting vertical and horizontal eddy diffusivities that are output in the model simulations. These values are also close to the values recommended by Bryan (2012) in order to produce realistic hurricane structure.

The fixed Coriolis parameter on an f-plane is 5×10^{-5} s^{-1} (*fcor=0.00005*).

The sea-surface temperature is 26.14 C (*tsurf=299.29*) with environmental surface pressure of 1015.1 mb (*psurf=101510.0*). The use of a simple bulk aerodynamic drag scheme (*idrag=1*) requires the use of a no-slip lower and upper boundary condition (*bcturbu=3*) setting; the treatment by the bulk aerodynamic scheme of the lower boundary in the CM1 code overrides the no-slip condition there.

A zero-flux condition is imposed at the top and bottom boundary for scalars (*bcuturbs=1*); the treatment by the bulk exchange scheme of the lower boundary in the CM1 code (*isfcflx=1*) overrides the zero-flux condition. For simplicity, we employ constant values for the drag coefficient ($C_{\rm D}$) and exchange coefficient (C_k)(*cecd=1*): $C_{\rm D} = 2.58 \times 10^{-3}$ and $C_k = 1.29 \times 10^{-3}$ (*cnstcd=0.00258, cnstce=0.00129*). The value for C_k is close to the mean value (1.2×10^{-3}) derived from the Coupled Boundary Layers/Air-Sea Transfer (CBLAST) experiment (Fig. 6 of Black et al. (2007); Fig. 4 of Zhang et al. (2009)), a recent laboratory study (Fig. 1 of Haus et al. (2010)) near and slightly above marginal hurricane wind speeds, and an energy and momentum budget analysis of the lower-tropospheric eyewall region at major hurricane wind speeds (Bell et al. 2012b). The value C_D is set to be twice the enthalpy exchange coefficient $C_{\rm D} = 2 \times C_k = 2.58 \times 10^{-3}$, and is close to the estimated mean value of $C_{\rm D} = 2.4 \times 10^{-3}$ from observations derived from CBLAST for major hurricane wind speeds by Bell et al. (2012b).

Open radiative boundary conditions are used on the lateral boundaries (*wbc=2, ebc=2, sbc=2, nbc=2*) employing the Durran and Klemp (1982) scheme (*irbc=4*); the outward flux is not restricted (*roflux=0*).

Rayleigh damping is applied at the upper boundary (*irdamp=1*) above a height of 20 km (*zd=20000.0*) with an inverse e-folding time scale of $1/300$ s^{-1} (*rdalpha=3.333e-3*). Rayleigh damping is turned off at the lateral boundaries (*hrdamp=0*). Dissipative heating is not included (*idiss=0*).

The simple Rotunno and Emanuel (1987) rainfall scheme is used (*ptype=6*) with a fixed fall speed of 7 m s^{-1} (*v_t=7.0*). Positive definiteness of moisture is ensured by a redistribution of moisture from neighboring cells (*pdscheme=1*).

As an expedient for radiative cooling, we follow Rotunno and Emanuel (1987) and choose simple Newtonian relaxation to the initial basic state sounding of potential temperature (*rterm=1*).

The initial vortex (Fig. 6) is provided in the public distribution of CM1v14, using name list option *iinit=7*. We use parameters for the nominal maximum tangential wind $V = 15$ m s^{-1}, the nominal radius of maximum tangential wind $R = 82.5$ km (although in practice the wind maximum is slightly weaker and the radius of maximum tangential wind is larger than the nominal values), the outer radius $R_0 = 412.5$ km, and the upper height for the vortex of $Z = 20$ km. The initial vortex is defined over the region $(r < R_0, z < Z)$ by

$$v(r,z) = \frac{Z-z}{Z}\left\{\sqrt{V^2\frac{r}{R}\left[G(r)+\frac{f^2r^2}{4}\right]}-\frac{fr}{2}\right\}, \tag{21}$$

where

$$G(r) = \left(\frac{2R}{r+R}\right)^2 - \left(\frac{2R}{R_0+R}\right)^2 \tag{22}$$

The basic state sounding is specified from an input file (*isnd=7*). The sounding used is obtained following the method of Rotunno and Emanuel (1987) for producing a near-neutral sounding.

References

Bell, M. M., M. T. Montgomery, and K. A. Emanuel, 2012a: Air-sea enthalpy and momentum exchange atmajor hurricane wind speeds observed during CBLAST. *J. Atmos. Sci.*, **69**, 3197–3222.

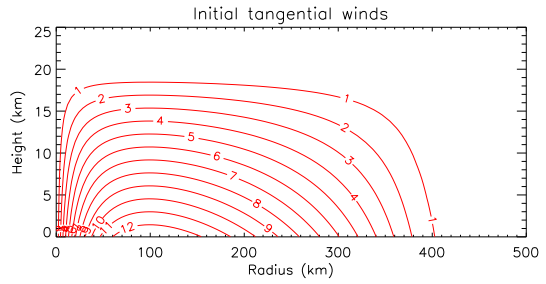

Figure 6. The initial tangential wind field (m s^{-1}) used in all numerical experiments presented.

Bell, M. M., M. T. Montgomery, and W. C. Lee, 2012b: An axisymmetric view of concentric eyewall evolution in Hurricane Rita (2005). *J. Atmos. Sci.*, **69**, 2414–2432.

Bister, M., and K. A. Emanuel, 1998: Dissipative heating and hurricane intensity. *Meteor. Atmos. Phys.*, **50**, 233–240.

Black, P. G., and Coauthors, 2007: Air-sea exchange in hurricanes. Synthesis of observations from the coupled boundary layer air-sea transfer experiment. *Bull Amer. Meteor. Soc.*, **88**, 357–374.

Bryan, G. H., 2012: Effects of surface exchange coefficients and turbulence length scales on the intensity and structure of numerically simulated hurricanes. *Mon. Wea. Rev.*, **140**, 1125–1143.

Bryan, G. H., and J. M. Fritsch, 2002: A benchmark simulation for moist non-hydrostatic numerical model. *Mon. Wea. Rev.*, **130**, 2917–2928.

Chavas, D. R., and N. Lin, 2016: A model for the complete radial structure of the tropical cyclone wind field. Part II: Wind field variability. *J. Atmos. Sci.*, **73**, early view.

Cushman-Roisin, B., 1994: *Introduction to Geophysical Fluid Dynamics*. Prentice Hall, 320 pp.

Drazin, P. G., and W. H. Reid, 1981: *Hydrodynamic Stability*. Cambridge University Press, Cambridge, England, 527pp.

Durran, D. K., and J. B. Klemp, 1982: On the effects of moisture on the Brunt-Väisälä frequency. *J. Atmos. Sci.*, 2152–2158.

Emanuel, K. A., 1986: An air-sea interaction theory for tropical cyclones. Part I: Steady state maintenance. *J. Atmos. Sci.*, **43**, 585–604.

Emanuel, K. A., 1988: The maximum intensity of hurricanes. *J. Atmos. Sci.*, **45**, 1143–1155.

Emanuel, K. A., 1995: Sensitivity of tropical cyclone to surface exchange coefficients and a revised steady-state model incorporating eye dynamics. *J. Atmos. Sci.*, **52**, 3969–3976.

Emanuel, K. A., 1997: Some aspects of hurricane inner-core dynamics and energetics. *J. Atmos. Sci.*, **54**, 1014–1026.

Emanuel, K. A., 2012: Self-stratification of tropical cyclone outflow. Part II: Implications for storm intensification. *J. Atmos. Sci.*, **69**, 988–996.

Emanuel, K. A., 2017: Will global warming make hurricane forecasting more difficult? *Bull. Amer. Meteor. Soc.*, **98**, 495–501.

Emanuel, K. A., and R. Rotunno, 2011: Self-stratification of tropical cyclone outflow. Part I: Implications for storm structure. *J. Atmos. Sci.*, **68**, 2236–2249.

Haus, B. K., D. Jeong, M. A. Donelan, J. A. Zhang, and I. Savelyev, 2010: Relative rates of sea-air heat transfer and frictional drag in very high winds. *Geophys. Res. Lett.*, **37**, doi:10.1029/2009GL042206, l07802.

Holton, J. R., 2004: *An Introduction to Dynamic Meteorology, 4th Edition*. Academic Press, London, 535pp.

Klemp, J. B., and R. B. Wilhelmson, 1978: The simulation of three-dimensional convective storm dynamics. *J. Atmos. Sci.*, **35**, 1070–1096.

Lilly, D. K., 1962: On the numerical simulation of buoyant convection. *Tellus*, **14**, 148–172.

Montgomery, M. T., S. V. Nguyen, R. K. Smith, and J. Persing, 2009: Do tropical cyclones intensify by WISHE? *Quart. Journ. Roy. Meteor. Soc.*, **135**, 1697–1714.

Montgomery, M. T., and R. K. Smith, 2014: Paradigms for tropical cyclone intensification. *Aust. Met. Ocean. Soc. Journl.*, **64**, 37–66.

Montgomery, M. T., and R. K. Smith, 2017: Recent developments in the fluid dynamics of tropical cyclones. *Annu. Rev. Fluid Mech.*, **49**, 541–574.

Nguyen, V. S., R. K. Smith, and M. T. Montgomery, 2008: Tropical-cyclone intensification and predictability in three dimensions. *Quart. Journ. Roy. Meteor. Soc.*, **134**, 563–582.

Persing, J., M. T. Montgomery, J. McWilliams, and R. K. Smith, 2013: Asymmetric and axisymmetric dynamics of tropical cyclones. *Atmos. Chem. Phys.*, **13**, 12 299–12 341.

Persing, J., M. T. Montgomery, R. K. Smith, and J. McWilliams, 2018: Quasi-steady hurricanes revisited. *Tropical Cyclone Science Reviews*, in press.

Rotunno, R., and K. A. Emanuel, 1987: An air-sea interaction theory for tropical cyclones. Part II Evolutionary study using a nonhydrostatic axisymmetric numerical model. *J. Atmos. Sci.*, **44**, 542–561.

Smagorinsky, J., 1963: General circulation experiments with the primitive equations. I: The basic experiment. *Mon. Wea. Rev.*, **91**, 99–164.

Smith, R. K., M. T. Montgomery, and S. Vogl, 2008: A critique of Emanuel's hurricane model and potential intensity theory. *Quart. Journ. Roy. Meteor. Soc.*, **134**, 551–561.

Zhang, F., and K. A. Emanuel, 2016: On the role of surface fluxes and wishe in tropical cyclone intensification. *J. Atmos. Sci.*, **73**, 2011–2019.

Zhang, J., W. M. Drennan, P. B. Black, and J. R. French, 2009: Turbulence structure of the hurricane boundary layer between the outer rainbands. *J. Atmos. Sci.*, **66**, 2455–2467.

Zhang, J. A., F. D. Marks, M. T. Montgomery, and S. Lorsolo, 2011a: An estimation of turbulent characteristics in the low-level region of intense Hurricanes Allen (1980) and Hugo (1989). *Mon. Wea. Rev.*, **139**, 1447–1462.

Zhang, J. A., and M. T. Montgomery, 2012: Observational estimates of the horizontal eddy diffusivity and mixing length in the low-level region of intense hurricanes. *J. Atmos. Sci.*, **69**, 1306–1316.

Zhang, J. A., R. F. Rogers, D. S. Nolan, and F. D. Marks, 2011b: On the characteristic height scales of the hurricane boundary layer. *Mon. Wea. Rev.*, **139**, 2523–2535.